Icarus 222 (2013) 81–99

Contents lists available at SciVerse ScienceDirect

Icarus

journal homepage: www.elsevier.com/locate/icarus

3D modelling of the early martian climate under a denser CO_2 atmosphere: Temperatures and CO_2 ice clouds

F. Forget [a,*], R. Wordsworth [a], E. Millour [a], J.-B. Madeleine [a], L. Kerber [a], J. Leconte [a], E. Marcq [b] R.M. Haberle [c]

[a] LMD, Institut Pierre-Simon Laplace, Universit P. et M. Curie, BP 99, 75005 Paris, France
[b] LATMOS, Institut Pierre-Simon Laplace, 78280 Guyancourt, France
[c] NASA Ames Research Center, Space Science Division, MS 245-3, Moffett Field, CA 94035-1000, USA

ARTICLE INFO

Article history:
Received 4 April 2012
Revised 6 October 2012
Accepted 9 October 2012
Available online 30 October 2012

Keywords:
Mars
Atmospheres, Evolution
Mars, Climate
Mars, Polar caps
Mars, Surface

ABSTRACT

On the basis of geological evidence, it is often stated that the early martian climate was warm enough for liquid water to flow on the surface thanks to the greenhouse effect of a thick atmosphere. We present 3D global climate simulations of the early martian climate performed assuming a faint young Sun and a CO_2 atmosphere with surface pressure between 0.1 and 7 bars. The model includes a detailed radiative transfer model using revised CO_2 gas collision induced absorption properties, and a parameterisation of the CO_2 ice cloud microphysical and radiative properties. A wide range of possible climates is explored using various values of obliquities, orbital parameters, cloud microphysic parameters, atmospheric dust loading, and surface properties.

Unlike on present day Mars, for pressures higher than a fraction of a bar, surface temperatures vary with altitude because of the adiabatic cooling and warming of the atmosphere when it moves vertically. In most simulations, CO_2 ice clouds cover a major part of the planet. Previous studies had suggested that they could have warmed the planet thanks to their scattering greenhouse effect. However, even assuming parameters that maximize this effect, it does not exceed +15 K. Combined with the revised CO_2 spectroscopy and the impact of surface CO_2 ice on the planetary albedo, we find that a CO_2 atmosphere could not have raised the annual mean temperature above 0 °C anywhere on the planet. The collapse of the atmosphere into permanent CO_2 ice caps is predicted for pressures higher than 3 bar, or conversely at pressure lower than 1 bar if the obliquity is low enough. Summertime diurnal mean surface temperatures above 0 °C (a condition which could have allowed rivers and lakes to form) are predicted for obliquity larger than 40° at high latitudes but not in locations where most valley networks or layered sedimentary units are observed. In the absence of other warming mechanisms, our climate model results are thus consistent with a cold early Mars scenario in which nonclimatic mechanisms must occur to explain the evidence for liquid water. In a companion paper by Wordsworth et al. we simulate the hydrological cycle on such a planet and discuss how this could have happened in more detail.

1. Introduction

Spacecraft sent to Mars in recent years have revealed new evidence suggesting that the environmental conditions on early Mars were very different than those today, with liquid water flowing on the surface at least episodically. Geomorphological evidence of past water flow in ancient terrains includes valley networks (remnant of widespread fluvial activity) (Carr, 1996), extensive sedimentary layered deposits (including delta-like landforms) (Malin and Edgett, 2000, 2003) and erosion rate much higher than today affecting the most ancient landforms (Craddock and Maxwell, 1993). Satellite remote sensing and in situ analysis of the surface mineralogy have also revealed the local presence of minerals which require liquid water for their formation: clay/phyllosilicates (Poulet et al., 2005; Bibring et al., 2006; Ehlmann et al., 2011), sulfates (Gendrin et al., 2005; Squyres et al., 2004), opaline silica (Squyres et al., 2008), carbonate (Ehlmann et al., 2008; Boynton et al., 2009; Morris et al., 2010) and chloride (Osterloo et al., 2008).

All these observations have provided a wealth of information about early Mars. In particular, they suggest that the conditions strongly varied throughout the Noachian and Hesperian era. Nevertheless, we still do not know if the conditions suitable for liquid water were stable on long timescales, or if they were the consequence of episodic, possibly catastrophic events. What is clear is that the conditions which allowed such extensive alteration by

* Corresponding author.
E-mail address: forget@lmd.jussieu.fr (F. Forget).

0019-1035/$ - see front matter © 2012 Elsevier Inc. All rights reserved.
http://dx.doi.org/10.1016/j.icarus.2012.10.019

liquid water occurred early in the history of Mars and not later. In particular, the fact that some alteration minerals can still be observed today, although they formed several billion years ago and are easily transformed into other materials by, e.g., diagenesis, suggests that water has been very limited on the martian surface from soon after their formation until today (Tosca and Knoll, 2009). Similarly the majority of the valley networks are found almost exclusively in the highly cratered ancient southern highlands, which date back from the end of the heavy bombardment period some 3.5–3.8 Gyr ago (Fassett and Head, 2008).

Although the role of hydrothermalism (resulting from volcanism or impacts) with respect to atmospheric induced processes is not clear, climate conditions were certainly different on early Mars. It is possible that the atmosphere could have been thicker than today, providing an environment more suitable for liquid water thanks to a surface pressure well above the triple point of water, and possibly a greenhouse effect capable of warming the surface closer to the melting points at 0 °C. In analogy with Earth and Venus, even after taking into account the differences in size, it can be estimated that the initial inventory of volatiles on Mars included at least several bars of atmospheric gases, mostly CO_2 (see Haberle, 1998). On this basis, since the 1980s, many studies have been performed to characterize the possible climate on early Mars assuming a CO_2 atmosphere thicker than today, and taking into account the fact that according to stellar evolution models the Sun's luminosity at 3.8 Ga was 75% of its present value (e.g., Gough, 1981). Almost all of these studies were performed using one-dimensional (1-D) radiative convective models (see Section 2). Such a characterization has been challenging however, because of the complex CO_2 gas spectroscopy, the likely formation of CO_2 ice clouds in the atmosphere, and the four-dimensional aspects of a planetary climate. The primary goal of the present paper is to update these calculations using a full 3-D climate model including a parameterization of CO_2 ice clouds and state of the art spectroscopic data. In a companion paper (Wordsworth et al., 2012) we extend these calculations by including a model of the possible water cycle that takes into account the radiative effects of water vapor and clouds, and can predict precipitation and the formation of lakes and glaciers on early Mars. To start with, in Sections 2 and 3 we review previous work on modelling early Mars climate, and briefly discuss the possible early Mars atmosphere composition and thickness. Section 4 describes our Global Climate Model (GCM). The simulated climates for various pressures, cloud microphysics parameters, obliquity values, orbital parameters, and possible atmospheric dust loadings are analyzed in Section 5. Finally, in Section 6, we discuss our results and conclude.

2. Previous modelling studies

The climate modelling studies of early Mars performed before 1998 are reviewed in detail in Haberle (1998). By the end of 1980s the paradigm for early Mars climate was based on the results of Pollack et al. (1987). Using a 1-D radiative convective model, they had shown that a 5-bar gaseous CO_2 atmosphere would raise the global mean surface temperature to 0 °C, allowing "warm and wet" conditions (though large, 5 bars of CO_2 was still consistent with contemporary estimates of the available inventory). This scenario was later challenged when Kasting (1991) published his reanalysis of the Pollack et al. (1987) greenhouse calculations. Kasting used the same model, but took into account the fact that at higher pressures CO_2 can condense in the middle atmosphere. This seriously decreases the greenhouse effect because of the latent heat warming of the middle atmosphere. Furthermore Kasting suggested that the resulting CO_2 ice clouds would probably raise the planetary albedo and further cool the planet. However, still working with the same model, Forget and Pierrehumbert (1997) later showed that the inclusion of the CO_2 ice cloud radiative effect at both solar and thermal infrared wavelengths led to a net warming of the surface rather than a cooling. Indeed, assuming that the CO_2 ice cloud particles are larger than a few micrometers, they can readily scatter infrared radiation and reflect outgoing thermal radiation back to the surface. The resulting warming effect more than compensates for the albedo increase due to the clouds. These calculations were later confirmed by Mischna et al. (2000), who used a more sophisticated and accurate 1-D radiative–convective transfer model based on correlated k-distribution methods. They noted that CO_2 ice clouds could also cool the surface if they are low and optically thick, and concluded that "estimating the actual effect of CO_2 clouds on early martian climate will require three-dimensional models in which cloud location, height, and optical depth, as well as surface temperature and pressure, are determined self-consistently". Nevertheless, the physics of carbon dioxide clouds in a dense CO_2 atmosphere was further explored by Colaprete and Toon (2003) still using a 1-D atmospheric model, but including a detailed microphysical cloud model. They took into account laboratory studies by Glandorf et al. (2002) showing that high critical supersaturations are required for CO_2 cloud particle nucleation and that surface kinetic growth is not limited. Under such conditions, Colaprete and Toon (2003) predicted large carbon dioxide ice particles with radii greater than 500 μm, and thus low cloud opacities. Because of this, and because of the warming of the atmosphere associated with cloud formation, they estimated that the greenhouse effect of CO_2 clouds would probably be limited to 5–10 K surface warming.

All these studies took into account the radiative effect of CO_2 and water vapor. Postawko and Kuhn (1986) also explored the possible greenhouse effect of SO_2. Yung et al. (1997) resumed this investigation, and studied the radiative effect of a very small amount (0.1 ppmv) of SO_2 in a 2 bar CO_2 atmosphere in a 1D model. They showed that it would raise the temperature of the middle atmosphere by approximately 10 K, so that the upper atmosphere would globally remain above the condensation temperature of CO_2. Exploration of the impact of SO_2 was further motivated by the discovery of sulfate sediments in Mars' ancient terrains (Gendrin et al., 2005; Squyres and Knoll, 2005; Halevy et al., 2007). Johnson et al. (2008) investigated the impact of larger amount of sulfur volatiles (H_2S and SO_2 mixing ratios of 1–1000 ppmv) in a martian atmosphere of 50 and 500 mbar of CO_2 (with H_2O). For this purpose they used the 3D Mars Weather Research and Forecasting (MarsWRF) general circulation model (Richardson et al., 2007). Their control simulations, achieved with a pure CO_2 atmosphere or with $CO_2 + H_2O$ (but neglecting the radiative effects of CO_2 clouds or H_2O clouds) are of interest in the present paper for comparison. Calculations performed including the sulfur volatile influxes suggested that these gases could have been responsible for greenhouse warming up to 25 K above that caused by CO_2. However, Tian et al. (2010) showed that such large amounts of SO_2 would inevitably lead to the formation of sulfate and large reduced sulfur aerosols (S_8). They concluded that these aerosols would have raised the planetary albedo and that the resulting cooling would more than outweigh the gaseous greenhouse effect.

In this paper, we do not include the effect of sulfur volatile and aerosols. Our goal is to investigate the details of the climate induced by a CO_2 atmosphere as simulated with a 3D Global Climate Model in which CO_2 cloud location, height, and optical depth, as well as surface temperature and pressure, are determined self-consistently for the first time. In comparison to the previous studies mentioned above, we also benefit from an improved parameterization of the collision-induced absorption of CO_2 (important for pressure larger than a fraction of a bar) that we have developed for this project, as described in Wordsworth et al. (2010) (see

details in Section 4.2). To calculate the collision-induced opacity in a CO_2 atmosphere, all the studies mentioned above relied without modification on a parameterization originally derived for the Venus atmosphere by James Pollack (Pollack et al., 1980; see detailed description in Kasting et al. (1984)). It was based on the measurements of Ho et al. (1971) from 7 to 250 cm^{-1}, and on a simple parameterization of collision induced opacity in the other spectral domains described in an unpublished PhD thesis by Moore (1971), still available as a NASA report. This parameterization included significant opacities between 526 and 295 cm^{-1} resulting from the pressure induced wings of the strong 15 μm bands. Unfortunately, this feature was kept in subsequent models, despite the fact that these opacities were probably overestimated and, in most cases, already accounted for in the codes chosen to calculate the radiative transfer in the 15 μm band. As a result, most previous studies probably overestimated the greenhouse warming of CO_2 by several kelvins.

3. Which atmosphere for early Mars?

By scaling the Earth or Venus volatile inventory, one can estimate that the amount of CO_2 brought to Mars during accretion was probably larger than 10 bars. However, Tian et al. (2009) showed that the extreme ultraviolet flux from the young Sun was so high that it would have strongly warmed the thermosphere and induced thermal escape of a primordial CO_2-dominated martian atmosphere. In their calculation, a CO_2 atmosphere could not have been maintained until about 4.1 byr ago. Under such conditions, how much atmosphere could have been degassed late enough after 4.1 Ga during the mid to late Noachian? Phillips et al. (2001) estimated that the total release of gases from the magmas that formed Tharsis during the Noachian era could have produced the integrated equivalent of a 1.5-bar CO_2 atmosphere. However, they assumed a magmatic CO_2 content of 0.65 wt.%, consistent with Hawaiian basaltic lavas. Since then, several authors have suggested that this was probably overestimated. In particular, Hirschmann and Withers (2008) calculated that post-4.5 Ga magmatism could have provided only 0.1 to at most 1 bar of CO_2. To refine these conclusions, Grott et al. (2011) combined the Hirschmann and Withers (2008) model for the solubility of CO_2 with a thermo-chemical evolution model to self consistently calculate the dissolved amount of CO_2 in martian magmas. They estimated that during Noachian, about 250 mbar of CO_2 were outgassed between 4.1 and 3.7 Ga.

In spite of these studies, if one assumes that more than 1 bar of atmospheric CO_2 was present during the Noachian era, where did it go? Estimating the amount of atmosphere that could have escaped to space in the last 4 Gyr is difficult because many different processes may have been involved, including photochemical escape, ions dragged by the solar wind field, sputtering, impact erosion, etc. (Chassefière and Leblanc, 2004). Up to now, only the present-day Mars ion loss by solar wind interaction has been measured, and found to be very small (Barabash et al., 2007). The possible loss of volatiles resulting from large impacts (Melosh and Vickery, 1989) is also difficult to model and constrain, but recent studies suggest that it must have been small (Pham et al., 2011). Altogether, the most recent estimations of the amount of CO_2 lost to space in the past 3.5 Gyr are below a few hundreds of millibars (Leblanc and Johnson, 2002; Lammer et al., 2008; Lammer, 2010).

Alternatively, one classical hypothesis is to assume that, as on Earth, large amounts of CO_2 could be stored in form of carbonates in the martian crust after chemical precipitation. However, almost no carbonates were initially detected by the OMEGA imaging spectrometer in spite of its high sensitivity to the spectral signature of carbonates (Bibring et al., 2005). Recently, several observations from orbiters (Ehlmann et al., 2008) and landers (Boynton et al., 2009; Morris et al., 2010) have revived the carbonate hypothesis and reasserted the importance of carbon dioxide in martian climate history (Harvey, 2010).

In this paper, we have chosen to explore the possible climate on early Mars for a wide range of surface pressures, up to 7 bars, as assumed in previous works on the same topic. However, when interpreting our model results, it is important to keep in mind that atmospheres thicker than 1 bar may be unlikely.

Another issue for an early Mars CO_2 atmosphere is its photochemical stability. Using a 1-D photochemical model of the martian atmosphere, Zahnle et al. (2008) showed that in a thick, cold and dry CO_2 atmosphere in which a surface sink is assumed for reactive oxidized gases (like H_2O_2 and O_3), CO_2 would tend to be reduced into CO. They noted that the process is very slow, and that "CO_2 atmospheres can be unstable but persistent simply because there isn't time enough to destroy them".

Finally, in this work we did not take into account the presence of other possible greenhouse gases. Such gases are not expected to be photochemically stable since they should have been photodissociated or oxidized, but they may be present if geochemical sources were active enough. This is further discussed in Section 6.3.

4. Global Climate Model description

4.1. Generalities

We have used a new "generic" version of the LMD Global Climate Model recently developed to simulate any kind of atmosphere with the goal of studying early climates in the Solar System (this paper) as well as possible climates on extrasolar planets (e.g. Wordsworth et al., 2011b). In practice, the model is derived from the LMD present-day Mars GCM (Forget et al., 1999), with several new parameterizations (see below and Wordsworth et al. (2012)). This Mars GCM has been used successfully to simulate Mars meteorology (e.g. Forget et al., 1998; Montmessin et al., 2004; Madeleine et al., 2011) and photochemistry (Lefèvre et al., 2004, 2008) from the surface to the thermosphere, and to simulate recent climate changes induced by the oscillations of Mars' rotational and orbital parameters (Levrard et al., 2004; Forget et al., 2006; Montmessin et al., 2007a, Madeleine et al., 2009). The LMD GCM solves the primitive equations of meteorology using a finite difference dynamical core on an Arakawa C grid. This dynamical core has been used and tested successfully in many kind of atmospheres thicker than present-day Mars such as the Earth (e.g. Hourdin et al., 2004), Venus (Lebonnois et al., 2010), and Titan (Hourdin et al., 1995; Lebonnois et al., 2012).

In this paper, simulations were performed with two horizontal resolutions: 32×24 (corresponding to resolutions of 7.5° latitude by 11.25° longitude) and 64×48 (3.75° latitude by 5.625° longitude). In the vertical, the model uses hybrid coordinates, that is, a terrain-following σ coordinate system near the surface and lower atmosphere (σ is pressure divided by surface pressure), and pressure levels in the upper atmosphere. In this work, with the exception of one sensitivity study described in Section 5.2, we used 15 layers with the lowest mid-layer levels at about 18 m, 60 m, 150 m, 330 m, 640 m, etc., and the top level at 0.3% of the surface pressure, that is about 5.3 scale heights (>50 km) above the zero datum.

Nonlinear interactions between explicitly resolved scales and subgrid-scale processes are parameterized by applying a scale-selective horizontal dissipation operator based on an n time iterated Laplacian Δ^n. This can be written $\partial q/\partial t = ([-1]^n/\tau_{\mathrm{diss}})(\delta x)^{2n}\Delta^n q$, where δx is the smallest horizontal distance represented in the model, τ_{diss} is the dissipation timescale for a structure of scale δx, and q a variable like temperature, meridional wind, or zonal wind.

As in most GCMs, such a dissipation operator is necessary to ensure the numerical stability of the dynamical core. However, it must be used with moderation (i.e. the dissipation timescales must be kept as high as possible). In particular, during this study we found that, when used with large topography variations and with atmospheric pressure larger than about 1 bar, our dissipation scheme tended to artificially produce some heat in the lower atmosphere. This production is usually completely negligible, but with high pressure and a strong greenhouse effect like in some of our simulations we found that the impact on surface temperatures could be non-negligible if the dissipation timescale were chosen smaller than necessary. This meant that our initial results overestimated the warming possible due to CO_2 clouds in the early martian atmosphere, and hence the likelihood of warm, wet conditions under a pure CO_2 atmosphere (Wordsworth et al., 2011a). Fortunately, we have been able to identify this issue, reduce the dissipation, and demonstrate that this problem does not affect the energy balance of the results presented in this paper.

Subgrid-scale dynamical processes including turbulent mixing and convection are parameterized as in Forget et al. (1999). In practice, the boundary layer dynamics are accounted for by Mellor and Yamada's (1982) unstationary 2.5-level closure scheme plus a "convective adjustment" which rapidly mixes the atmosphere in the case of unstable temperature profiles. Turbulence and convection mixes energy (potential temperature), momentum (wind), and tracers (gases and aerosols). The subgrid-scale orography and gravity wave drag schemes of the present-day Mars GCM (Forget et al., 1999) were not applied.

Surface temperature evolution is governed by the balance between radiative and sensible heat fluxes (direct solar insolation, thermal radiation from the atmosphere and the surface, and turbulent fluxes) and thermal conduction in the soil. The parameterization of this last process is based on an 18-layer soil model solving the heat diffusion equation using finite differences. The depth of the layers were chosen to capture diurnal thermal waves as well as the deeper annual thermal wave. A vertically homogeneous soil is assumed. For most simulations, the thermal inertia is set to 250 J $s^{-1/2}$ m^{-2} K^{-1} everywhere (a value slightly higher than the mean value on present-day Mars, to account for the higher gaseous pressure in the pore space which increase the soil conductivity). For the ground albedo, as well as for the topography, we chose to keep the same distributions as observed on Mars today. We realize that both fields may have been quite different 3 byr ago, but we assume that the present-day values can be representative of the range and variability of the Noachian–Hesperian eras. In Section 5.1, the sensitivity of our results to surface thermal inertia and albedo is discussed.

4.2. Radiative transfer in a thick CO_2 atmosphere

Our radiative scheme is based on the correlated-k model, with the absorption data calculated directly from high resolution spectra computed by a line-by-line model from the HITRAN 2008 database (Rothman et al., 2009). These were then converted to correlated-k coefficients for use in the radiative transfer calculations.

In practice, at a given pressure and temperatures, correlated-k coefficients in the GCM are interpolated from a matrix of coefficients stored in a 6×9 temperature and log-pressure grid: $T = 100,\ 150,\ 200,\ 250,\ 300,\ 350$ K, $p = 10^{-1}, 10^{0}, 10^{1}, \ldots, 10^{7}$ Pa. We used 32 spectral bands in the thermal infrared and 36 at solar wavelengths. Sixteen points were used for the g-space integration, where g is the cumulated distribution function of the absorption data for each band. Rayleigh scattering by CO_2 molecules was included using the method described in Hansen and Travis (1974), and using the Toon et al. (1989) scheme to compute the radiative transfer.

As mentioned in Section 2, a key improvement of our radiative transfer model compared to previous models is the use of an improved parameterization for the CO_2 collision-induced absorption (CIA). It was specially developed for the present study using the results of Baranov et al. (2004) and Gruszka and Borysow (1998). The method is described and justified in Wordsworth et al. (2010). The sublorentzian profiles of Perrin and Hartmann (1989) were used for the CO_2 far line absorption.

4.3. CO_2 ice condensation and clouds

The model includes a parameterization to account for the possible condensation of CO_2 when temperatures fall below the condensation temperature T_c. To compute T_c as a function of pressure p (Pa), we used the expression provided by Fanale et al. (1982):

$$T_c = -3167.8/[\ln(0.01p) - 23.23] \quad (1)$$

for $p < 518{,}000$ Pa,

$$T_c = 684.2 - 92.3\ln(p) + 4.32\ln(p)^2 \quad (2)$$

for $p > 518{,}000$ Pa (518,000 Pa is the pressure of the triple point of CO_2).

As on Mars today, CO_2 can directly form on the ground: When the surface temperature falls below the condensation temperature, CO_2 condenses, releasing the latent heat required to keep the solid–gas interface at the condensation temperature. Conversely, when CO_2 ice is heated, it partially sublimates to keep its temperature at the frost point. When CO_2 ice is present, the surface albedo and emissivity are set to 0.5 and 0.85 respectively. On present-day Mars, this albedo varies a lot in space and time. 0.5 is consistent with the various estimation of the average CO_2 ice cap albedo used to fit the seasonal pressure variations induced by the condensation and sublimation in the polar caps (Forget et al., 1998; Haberle et al., 2008).

In our simulations, CO_2 ice clouds also form in the atmosphere. Such clouds have been observed on present-day Mars during the polar night in the lower atmosphere (see e.g. Pettengill and Ford, 2000; Tobie et al., 2003) and in the equatorial mesosphere around 60–80 km (Montmessin et al., 2007b; Määttänen et al., 2010). These mesospheric CO_2 ice clouds may share some similarities with those predicted in our early Mars simulations. However they form more rarely (probably because the atmosphere is not often below the frost point (González-Galindo et al., 2010; Forget et al., 2009)) and at significantly lower pressures (0.1–0.01 Pa). In spite of this, the observed optical depths and particle radii are large (typically around 0.2 and 3 μm, respectively), suggesting that the growth of CO_2 ice particles in a CO_2 gas atmosphere is a very efficient process.

In theory, to properly model the formation of such clouds, one must take into account various microphysical processes such as supersaturation, nucleation and crystal growth (Wood, 1999; Colaprete and Toon, 2003). In most of our simulations, however, we assumed that condensation would occur as soon as the temperature T^* predicted from the dynamical and radiative cooling rates dropped below T_c. In Section 5.3, we also present results from a test case in which a 30% supersaturation is required before condensing.

At each timestep, the mass mixing ratio m (kg/kg) of condensed ice in a model box (or its evolution δm if ice is already present) is simply deduced from the amount of latent heat needed to keep $T = T_c$:

$$\delta m = \frac{c_p}{L}(T_c - T^*) \quad (3)$$

with δm the mass mixing ratio of ice that has condensed or sublimed (>0 when condensing), c_p the specific heat at constant pressure (we took 735.9 J kg^{-1} K^{-1}) and L the latent heat of CO_2 (5.9×10^5 J kg^{-1}).

CO_2 ice is transported by the large scale circulation and by turbulent and convective mixing. The transport scheme used in our GCM is a "Van-Leer I" finite volume scheme (Hourdin and Armengaud, 1999).

To estimate the size of the cloud particles, we assumed that the number mixing ratio of cloud condensation nuclei [CCN] (kg^{-1}) is constant throughout the atmosphere. Assuming that the cloud particle size distribution is monodisperse in each box, the cloud particle radius r is then given by:

$$r = \left(\frac{3m}{4\pi\rho[\mathrm{CCN}]}\right)^{1/3} \quad (4)$$

with ρ the CO_2 ice density, set to 1620 kg m^{-3} in our model.

Once r is known, the cloud particle sedimentation velocity w is calculated using Stokes law (Rossow, 1978). Sedimentation is then computed separately from the transport, but using a similar Van-Leer I transport scheme in the vertical.

Sedimentation and condensation are strongly coupled. Within one physical timestep (1/48 of a sol, or 1850 s in our model), we found that a significant part of the ice that forms within a cloud can sedimentate to the layers below, where it can condense at a different rate or even sublimate. For these reasons, in the model, condensation and sedimentation schemes are coupled together and integrated with a sub-timestep equal to 1/20 of the physical timestep.

The cloud particle sizes are also used to calculate the cloud radiative effect. Refractive indices for CO_2 ice are taken from Hansen (2005) and Mie theory is assumed to retrieve the single scattering properties. Scattering and absorption are computed at both solar and thermal infrared wavelengths using the Toon et al. (1989) scheme.

[CCN] is clearly a key parameter which directly controls the properties and the impact of the modelled clouds. Exploring the sensitivity of the results to this poorly known parameter allows us to account for most of the uncertainties related to the CO_2 ice clouds microphysics and particles size distribution. What is the possible range of [CCN]? On the Earth, the number mixing ratio of cloud condensation nuclei in the troposphere ranges between 10^6 kg^{-1} (for low saturation in clean polar air) and 10^{10} kg^{-1} (polluted air mass) (Hudson and Yum, 2002; Andreae, 2009). It is significantly lower for icy cirrus clouds (<10^4 kg^{-1}) (e.g. Demott et al., 2003) . Even in the absence of surface or chemical sources, a minimum number of nuclei would be provided by meteoritic dust and smoke particles which have been suggested to be possible condensation nuclei for terrestrial Polar Mesospheric Clouds (Gumbel and Megner, 2009). Such particles must have been abundant 4 byr ago. In this paper, we explore [CCN] values ranging from 10^2 kg^{-1} to 10^8 kg^{-1}, with a baseline value of 10^5 kg^{-1}.

4.4. Atmospheric dust

Early Mars winds were probably able to lift and transport mineral dust from the surface. If the planet was dry enough, and in the absence of oceanic sinks as on the Earth, we must take into account the possibility that the atmosphere was laden with mineral aerosols, as on Mars today. To explore the impact of atmospheric dust on the early Mars climate, we added a second type of aerosol in addition to the CO_2 ice clouds particles. We assume that the dust is similar to that observed on present-day Mars and use Wolff et al. (2009) optical properties, with a constant effective radius of 1.5 μm. Instead of simulating the lifting and transport of dust by the winds, we prescribe the dust mixing ratio in the atmosphere and assume that it does not vary with time. The column averaged dust optical depth at the mean pressure level is horizontally uniform. In the vertical, the dust mixing ratio q is taken to be constant in the lower atmosphere up to a level above which it rapidly declines, as in Forget et al. (1999):

$$q = q_0 \exp\left\{0.007\left[1 - (p_0/p)^{(70\ \mathrm{km}/z_{\max})}\right]\right\} \quad p \leqslant p_0 \quad (5)$$

$$q = q_0 \quad p > p_0 \quad (6)$$

where q_0 is a constant determined by the prescribed optical depth at the global average surface pressure p_0, and $z_{\max}$ the altitude (km) of the top of the dust layer. In this paper simulations were performed with $z_{\max}$ = 30 and 100 km (see Section 5.5).

5. Results

To explore the range of climates that may have occurred on a planet like early Mars with a thick CO_2 atmosphere, we have performed multiple simulations with different values of key model parameters : (1) mean surface pressure, (2) cloud microphysics parameters (i.e. cloud condensation nuclei density), (3) obliquity and eccentricity, (4) surface properties, (5) atmospheric dust loading. The impact of water vapor is also discussed. Solar luminosity is set to 75% of the present value (see Section 6.2 for a discussion of this assumption). The solar spectrum was assumed to be the same as today. All results correspond to the last year of a 10-year simulation. In all cases, the modelled planet has reached equilibrium by this time (results are repeatable from year to year), except in the case of permanent CO_2 condensation, which induces a slow decrease of the atmospheric mass and pressure (atmospheric collapse; see below).

5.1. Surface temperatures and CO_2 ice caps

In this section, we describe simulations performed assuming a circular orbit, 25° obliquity like on present-day Mars, no dust, and a constant cloud condensation nuclei number density [CCN] set to 10^5 kg^{-1}.

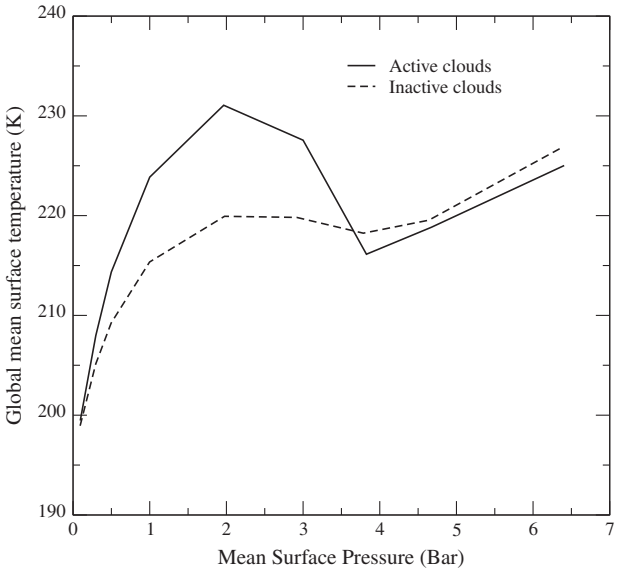

Fig. 1. Global mean annual mean surface temperature (K) as a function of surface pressure in our baseline simulations (obliquity = 25°, [CCN] = 10^5 kg^{-1}, circular orbit) with and without radiatively active CO_2 ice clouds.

Fig. 1 presents global/annual mean surface temperature (K) as a function of mean surface pressure *Ps*. Results obtained without taking into account the radiative effects of CO_2 ice clouds (the clouds are assumed to be "transparent" at all wavelengths) are in agreement with previous 1D model calculations performed with the same radiative transfer parameterization (Wordsworth et al., 2010). Surface temperature increases up to *Ps* = 2 bar. Above 2–3 bar Rayleigh scattering by CO_2 gas more than compensates for the increased thermal infrared opacity of the atmosphere. Increasing the atmospheric thickness does not result in an increase of the mean surface temperature. Taking into account the radiative effect of CO_2 ice clouds results in a global warming of the surface by more than 10 K resulting from the CO_2 ice cloud scattering greenhouse effect (Forget and Pierrehumbert, 1997). In the GCM, this effect is significant, but not as much as it could have potentially been according to the estimation by Forget and Pierrehumbert (1997). This is mostly because the cloud opacities remain relatively low compared to what was assumed in that study (see below). Fig. 2 shows the radiative budget corresponding to Fig. 1 simulations. One can see that the clouds strongly raise the planetary albedo and thus decrease the absorbed solar radiation. On this plot, one can verify that the absorbed solar energy is equal to the emitted infrared energy (i.e. the simulated planet is in radiative equilibrium as expected), except at high pressure when the atmosphere collapses on the surface and releases latent heat, as detailed below.

Fig. 3 presents the seasonal and latitudinal variation of zonal mean surface temperature and surface CO_2 ice for the different surface pressure experiments. The maximum accumulations of CO_2 ice is not found exactly at the poles because CO_2 ice clouds are predicted to be especially thick there, and their effect on the incident thermal infrared flux tend to limit the surface cooling and thus the surface condensation.

With $0.5 \leqslant Ps \leqslant 2$ bar, seasonal CO_2 ice caps are predicted to form at high latitudes during fall, winter and spring as in the Mars northern hemisphere today. For $Ps \leqslant 0.3$ bar, however, permanent surface CO_2 ice glaciers are predicted to form at high latitudes in both the radiatively active and inactive cloud cases. In these simulations, the atmosphere is collapsing and the results after 10 years may not represent a realistic long-term solution. Many more years would be required to reach a steady state in which the permanent CO_2 ice caps would be in solid–gas equilibrium with the atmosphere, with a significant part of the atmosphere trapped on the surface.

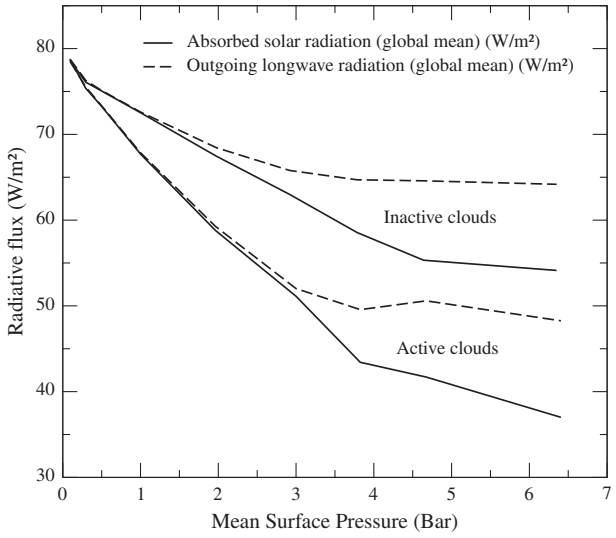

Fig. 2. Global mean annual mean radiative budget for the same simulations as in Fig. 1 with or without radiatively active clouds. After 10 years, simulations with surface pressure higher than 3 bars are out of equilibrium because of atmospheric collapse and the constant release of latent heat at the surface.

Fig. 4 shows maps of the extension of the permanent CO_2 caps after 10 and 25 years. Between 1 and 25 years, the atmospheric mass collapses by 1% per year in the (initially) 0.1-bar simulations, whereas the pressure drops by only 0.032% per year in the 0.3-bar case. To properly simulate an equilibrated atmosphere/permanent CO_2 ice cap system, it would also be necessary to take into account the ability of CO_2 ice glaciers to flow and spread (CO_2 ice is known to be much softer than H_2O ice at the same temperature (Kreslavsky and Head, 2011; Durham et al., 1999)), and probably to include the effect of slopes and roughness (Kreslavsky and Head, 2005).

The formation of permanent polar caps at low pressure is also very dependent on obliquity. This is discussed in detail in Section 5.4.

For $Ps \geqslant 3$ bar, permanent surface CO_2 ice glaciers are also predicted to form on the surface in both the radiatively active and inactive cloud cases. CO_2 ice tends to condense permanently in the colder areas at high altitudes and latitude. In the *Ps* = 3 bar case, the permanent CO_2 ice glaciers are restricted to a couple of locations on the Tharsis bulge near 30°S–100°W, and in the southern high latitudes around 75°S–100°E (Fig. 5a). For *Ps* = 4 bar and more, the permanent CO_2 ice sheets are much more extensive, covering high latitudes and most of the Tharsis bulge (Fig. 5b).

The fact that permanent CO_2 ice cap form at either low or high pressure can be interpreted as follows: At low pressures, the greenhouse effect and heat transport are weak and thus temperatures easily reach the frost point. At high pressures the increase in the frost point temperature overcomes the increased greenhouse effect and CO_2 also condense easily. In addition, heat transport is then so efficient that horizontal temperature gradients are small. Consequently, CO_2 ice can form in non-polar regions.

The formation of extensive permanent and seasonal polar caps at high pressures buffers the surface temperature and explains the increase of global mean surface temperature for $Ps \geqslant 4$ bar in Fig. 1. In these simulations, thick CO_2 ice clouds form just above the surface. Such clouds tend to cool the surface (Mischna et al., 2000) because they reflect solar radiation throughout their entire depth (the planetary albedo is increased) whereas only the upper layers can contribute to reflect the thermal infrared flux emitted by the atmosphere below them. As a result, the radiatively active clouds simulations show mean surface temperatures even lower than when the clouds are assumed to be transparent.

Fig. 6a and b presents annual mean surface temperature maps in the more realistic *Ps* = 0.5 and 2 bar cases. One can notice that surface temperatures strongly depend on the local topography, especially in the 2 bars simulations in which the lowest plains are the warmest places on Mars. This is not due to a stronger greenhouse warming where the atmosphere is thicker. As illustrated in Fig. 1, the increase of surface temperature with CO_2 pressure due to greenhouse effect is weaker at high pressure and negligible above 2 bars. The opposite is found in our maps.

In fact, Earthlings are familiar with this situation, which results from adiabatic cooling and warming of the atmosphere when it moves vertically and the fact that the atmosphere can influence the surface temperature when it is dense enough. On present-day Mars, the atmosphere is too thin to affect the surface temperature. The local topography has no significant effect on surface temperature. At which atmospheric pressure does the transition between a "present-day Mars regime" and an "Earth-like regime" occur? To address this question, we have computed the mean surface temperature lapse rate as a function of mean surface pressure (Fig. 7). The lapse rate is simply estimated by performing a linear regression between annual mean surface temperatures and ground altitude at every grid point for latitudes lower than 30°, to avoid the influence of seasonal CO_2 ice condensation. We can see that

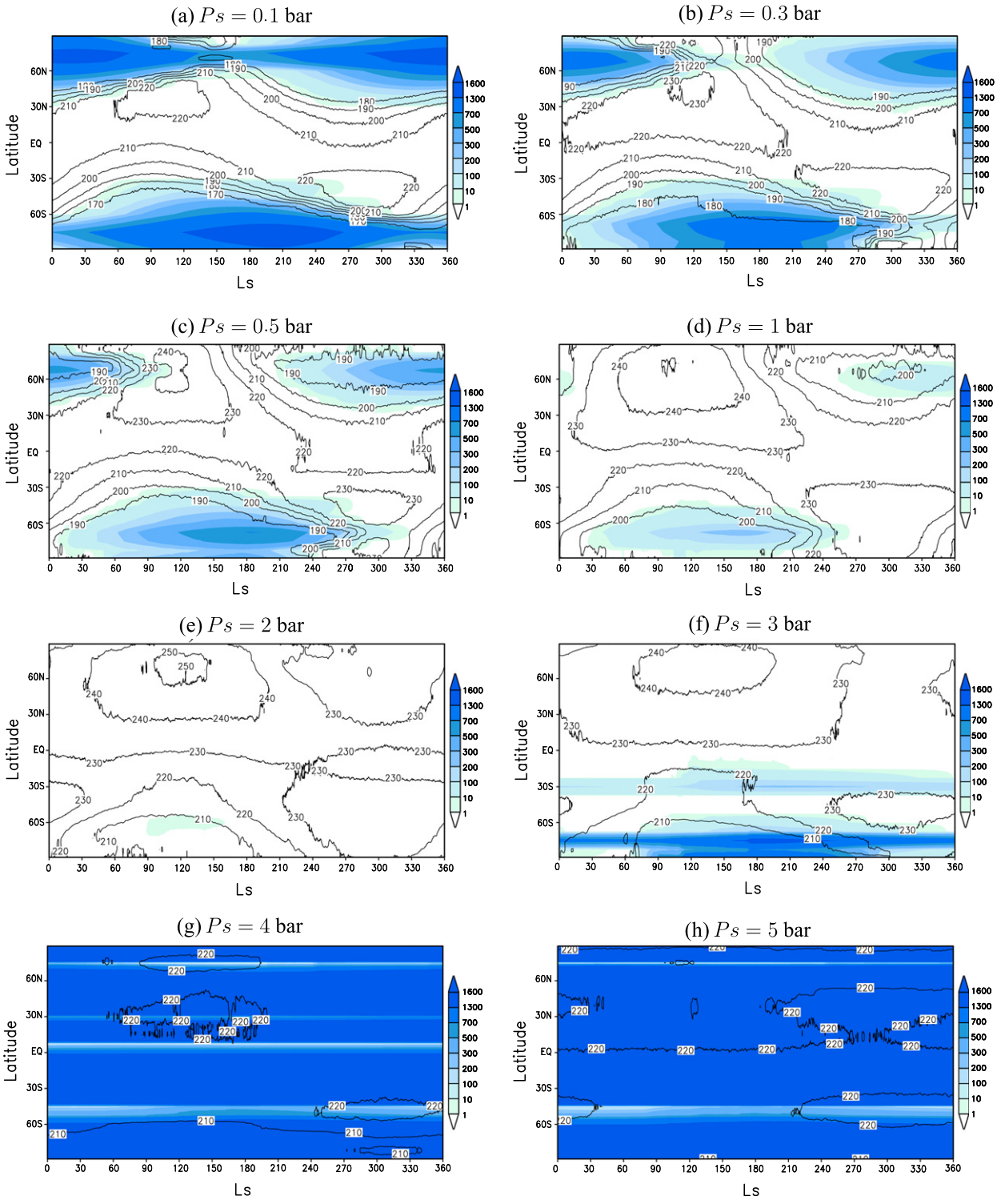

Fig. 3. Zonal mean surface temperatures (contours, K) and surface CO_2 ice (kg m^{-2}) as a function of solar longitude L_s (°) for various mean surface pressures *Ps* (obliquity = 25°, [CCN] = 10^5 kg^{-1}, circular orbit).

the surface temperature lapse rate quickly decreases with increasing pressure. The effect is already significant (−1.5 K/km) for *Ps* = 0.5 bar, and reaches an asymptotic value (−2.5 K/km) above about 2 bars. This is half the theoretical dry atmospheric lapse rate equal to −5.05 K/km in our model. This can be compared to the Earth case, where surface temperature lapse rates ranging between around −3 and −6.5 K/km have been reported (see Minder et al. (2010) and references therein), while the reference dry atmospheric lapse rate is −9.8 K/km. However on the Earth water condensation can decrease the lapse rate by a factor of two.

In our simulations, annual mean surface temperatures are always significantly below 0 °C. In theory, this means that potential oceans and near-surface groundwater should be permanently frozen in ice sheets and permafrost. Could surface lakes and rivers form? To investigate this possibility, a better criterion is the average temperature in summer. On the Earth, for instance, intense

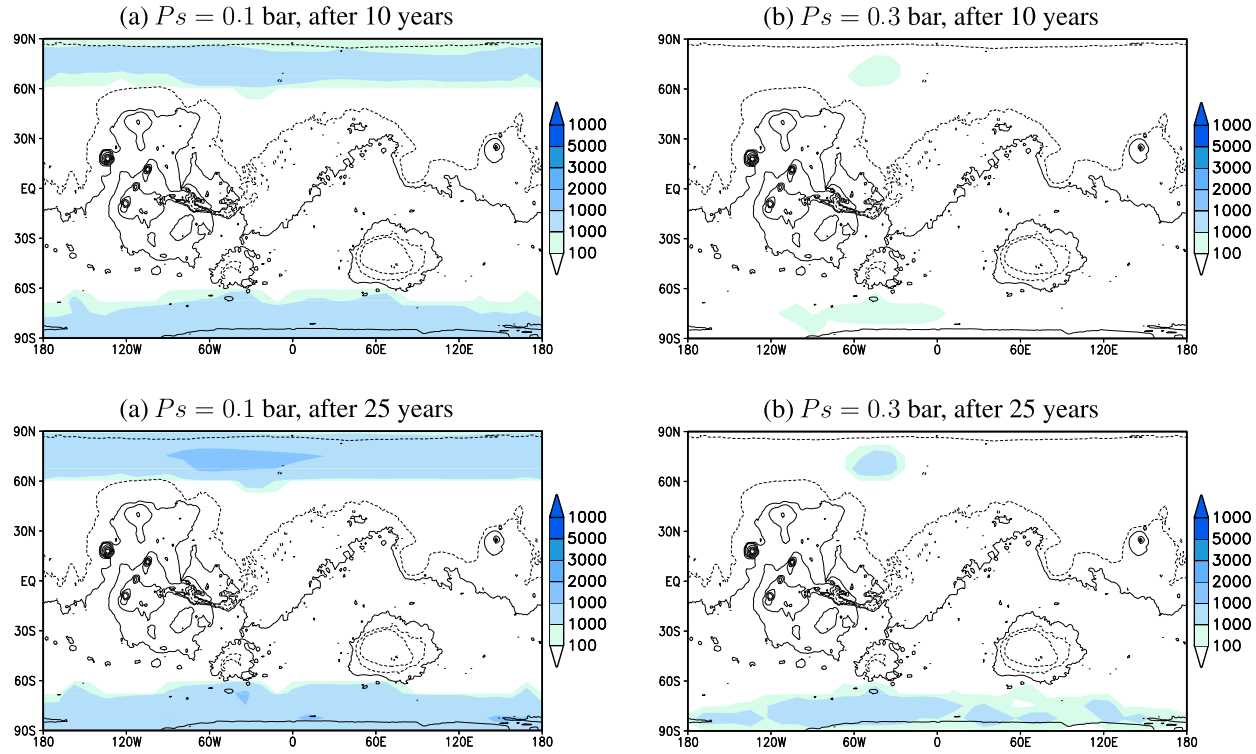

Fig. 4. Maps of the permanent surface CO_2 ice deposits (kg m^{-2}) for the *Ps* = 0.1 and *Ps* = 0.3 bar simulations, also shown in Fig. 3. In practice, these maps show the yearly minimum CO_2 ice mass recorded during the 10th and 25th simulated years, to show where the ice never sublimes during the year. Contours illustrate topography (contours below zero elevation are dotted).

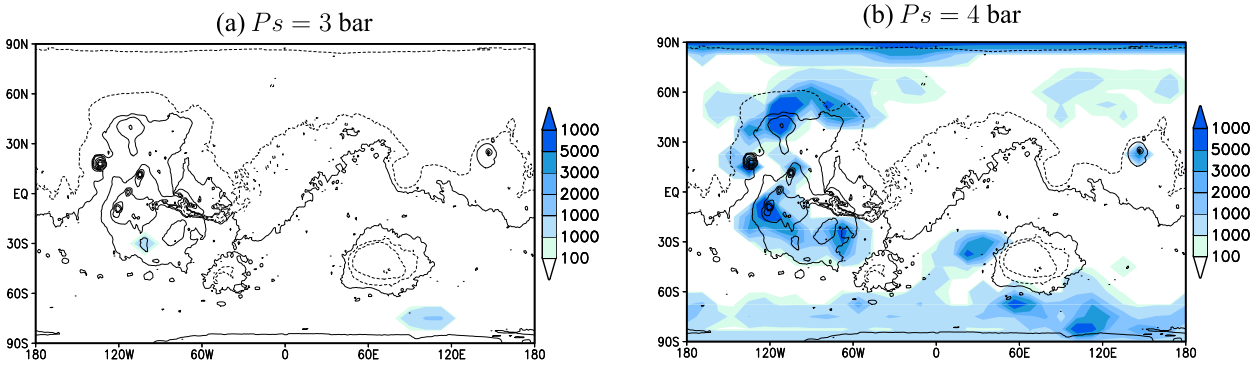

Fig. 5. Same as Fig. 4, but for *Ps* = 3 and 4 bar simulations also shown in Fig. 3. These show the yearly minimum CO_2 ice mass (kg m^{-2}) recorded during the 10th year of the simulation.

fluvial activity takes place in Northern Siberia in the summertime, despite annual mean surface temperatures below −15 °C (258 K). Maps of peak summertime daily mean temperatures are shown in Fig. 6c and d. It appears that, unlike those in Siberia, these temperatures never reach the melting point of pure water in our baseline simulations. In fact, the climate predicted by our model should be, at best, analogous to Antarctica's upper Dry Valleys (Marchant and Head, 2007). Water may melt, but only for a few hours during a few afternoons in summer (as on Mars today). The locations where above-freezing temperatures are predicted are shown in Fig. 6e and f, which presents the maximum surface temperatures in the *Ps* = 0.5 and 2 bar cases. Melting would be possible in many areas below 60° latitude. Although the mean temperatures are lower in the 0.5 bar than in the 2 bar simulation, the diurnal amplitude is larger and the maximum temperatures are not very dependent on pressure. The amount of water which can melt during such short episodes should be limited (see Wordsworth et al., 2012). One can speculate that the meltwater could create supraglacial channels below the glaciers, maintain perennially ice-covered lakes (notably by bringing energy in the form of the latent heat of fusion; McKay et al., 1985), or that brines may play a major role. However, one must keep in mind that in our baseline simulations we modelled a dry, desertic planet Mars. First, we do not take into account the latent heat losses which tend to cool the surface if ice were present. Second, surface ice could possibly have higher albedo and thermal inertia than bare ground. To assess the sensitivity of our results to surface properties and the presence of ice, we performed additional simulations with a global albedo of 0.4 (instead of the present day Mars ground albedo which is near 0.22 on average) and a global thermal inertia of 1000 J s$^{-1/2}$ m^{-2} K^{-1} (instead of

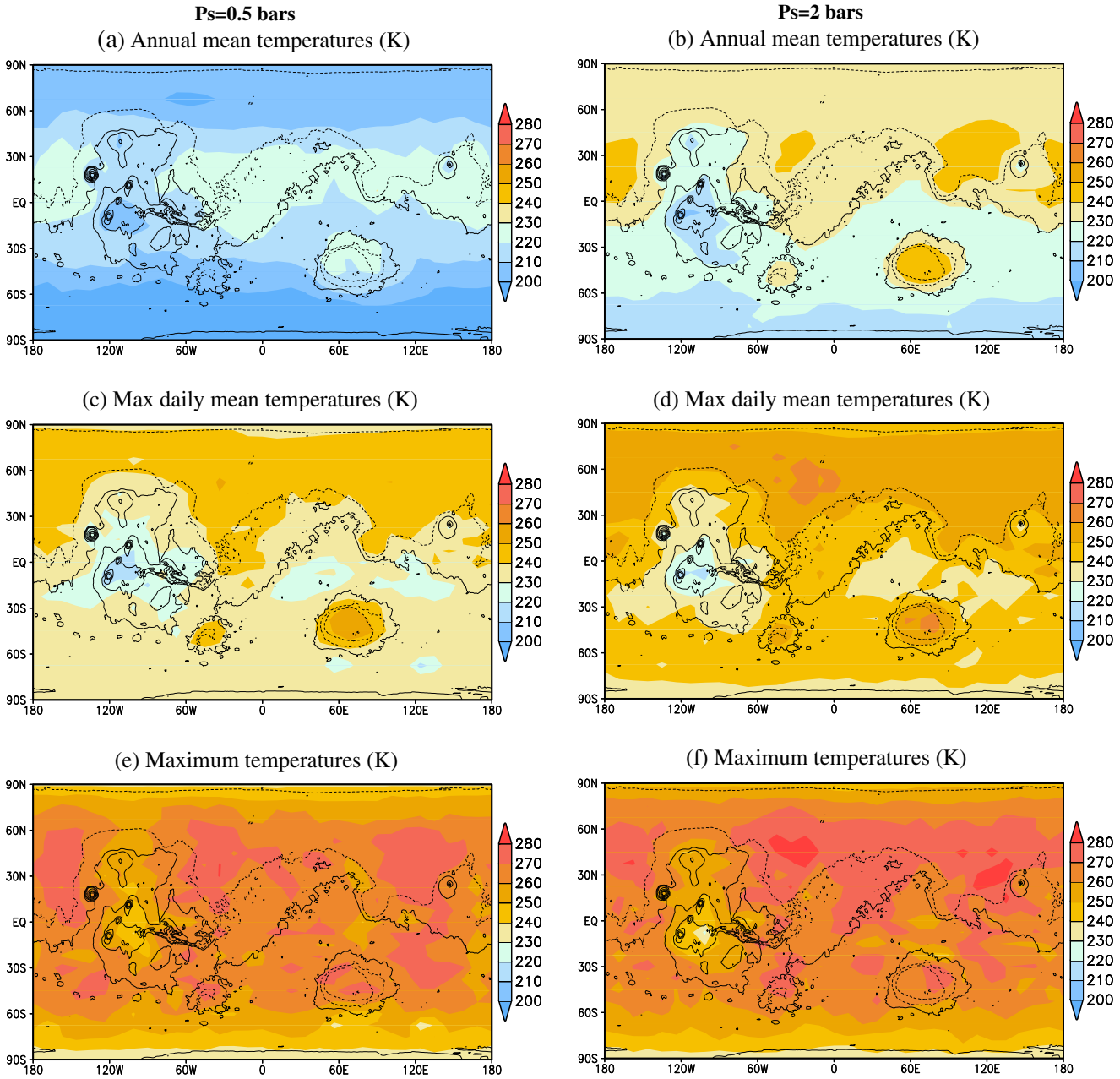

Fig. 6. Surface temperatures (K) in our baseline simulations (obliquity = 25°, [CCN] = 10^5 kg^{-1}, circular orbit) for mean surface pressure 0.5 bar and 2 bar. Ground albedo is as on present day Mars. Thermal inertia is set to 250 J s$^{-1/2}$ m^{-2} K^{-1} everywhere.

250 J s$^{-1/2}$ m^{-2} K^{-1} assumed for dry ground). As shown in Fig. 8, annual mean temperatures are lowered by about 8 and 12 K at 0.5 and 2 bar respectively. This reflects the effect of lowering the albedo, since thermal inertia has little effect on annual mean temperatures. However, increasing the thermal inertia dampens the maximum temperatures, which are lowered by about 30 K. This suggests that extensive ice deposits would not reach 0 °C, and that, as in Antarctica upper Dry Valleys today, only ice lying on dark rocks may sometimes melt (Marchant and Head, 2007).

5.2. Atmospheric temperatures and CO_2 ice clouds

Fig. 9 presents cross-sections of zonal mean temperatures and zonal winds in northern summer and winter in the 2 bar baseline simulation. At this pressure, the atmospheric thermal structure is relatively homogeneous, with little latitudinal and seasonal variations compared to present-day Mars or even the Earth. Temperatures decrease monotonically with altitude, even near the surface, as discussed above. The small latitudinal gradients nevertheless induce a meridional circulation. Plotting the mass streamfunction (not shown) reveals that it is characterized by Earth-like overturning Hadley cells between 30°S and 30°N, and which extend up to about 15 km. In a given season, the cross-equatorial cell with rising motion in the spring–summer hemisphere and descending motion in the fall–winter hemisphere dominates. The corresponding zonal wind structure is characterized by an Earth-like subtropical prograde jet in the winter hemisphere. The summer hemisphere retrograde jet is much more Mars-like. In the northern hemisphere, the large longitudinal variations in topography induce a strong stationary wave which modulates the zonal wind.

In this 2-bar simulation, temperatures below the CO_2 condensation point are predicted above about 11 km, and CO_2 ice clouds form at all seasons and latitudes (Fig. 10). However, at any given

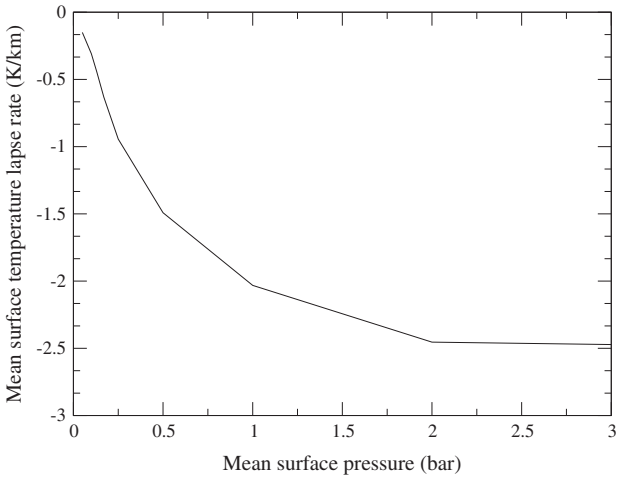

Fig. 7. Mean surface temperatures variation with topography (K/km) as a function of mean surface pressure (bar). This lapse rate is obtained by performing a linear regression between annual mean surface temperatures obtained below 30° latitude (to avoid the influence of the polar caps) and the local topography in our baseline cases (obliquity = 25°, [CCN] = 10^5 kg^{-1}, circular orbit).

time, CO_2 ice clouds typically cover about half of the planet (when counting visible opacity above 0.2), as illustrated in Fig. 11. The locations of the clouds evolve constantly, with a combination of transient clouds condensed and transported by travelling waves, and stationary clouds forming above topography features (such as Tharsis, the edge of Hellas or Arabia Terra). This most likely results from resolved gravity waves. Is topography a key driver of clouds and climate? To address this question, we performed a similar simulation, but with topography removed. We found that the cloud coverage is relatively similar, with a global mean visible opacity of 6 compared to 4.5 with topography. The mean surface temperature is almost identical (231.5 K compared to 231.0 K).

Fig. 10a and c shows the annual mean section of the cloud density and cloud particles radii in our 2-bar baseline simulation with topography. The average particle radius is well above 10 μm, the minimum size to readily scatter thermal infrared radiation and induce the scattering greenhouse effect (Forget and Pierrehumbert, 1997). However, with a mean optical depth near 4.5 and fractional cloud cover most of the time, the clouds only induce a 10 K greenhouse warming, as discussed above.

Because modelled clouds properties can be expected to be sensitive to model resolution, we performed an additional 2-bar simulation with doubled resolution in latitude and longitude. Results are compared in Figs. 10–12e and f. In the high-resolution simulation, the impact of topography and gravity waves seems to be stronger. The cloud distribution (Fig. 12f) exhibits more structure in relation to local topography. Nevertheless, the mean cloud cover, optical depth, and particle sizes are about the same on average (average visible opacity of 4.6 vs 4.5 in the baseline simulation). The mean surface temperature is only 1 K warmer, which is not significant. Similarly, we explored the sensitivity to the model vertical resolution by doubling the number of layers and thus the resolution above the boundary layer (reaching a vertical resolution of about 2.5 km between 5 and 25 km), and found very similar results.

Fig. 12 presents the annual mean coverage in optical depth at other pressures in the baseline cases. The average cloud visible optical depth τ growths with mean pressure Ps, but at the same time the altitude of the bottom of the cloud layer z decreases. For instance, $\tau = 0.7$ and $z \simeq 14$ km for $Ps = 0.5$ bar; $\tau = 1.8$ and $z \simeq 11$ km for $Ps = 1$ bar; $\tau = 4.5$ and $z \simeq 8$ km for $Ps = 2$ bar; $\tau = 9$ and $z \simeq 5$ km for $Ps = 3$ bar; and $\tau = 16$ and $z \simeq 0$ km for $Ps = 4$ bar. As mentioned above, the scattering greenhouse effect for low lying clouds is reduced. Above 4 bars, the clouds cool the planet rather than warming it.

5.3. Sensitivity to CO_2 ice cloud microphysics

5.3.1. Number of particles and particle sizes

As explained in Section 4.3, we consider that many of the uncertainties related to the CO_2 ice clouds microphysics and particle sizes can be accounted for by varying the prescribed number mixing ratio of cloud condensation nuclei [CCN]. We explored the sensitivity of the model to this parameter in the $Ps = 0.5$ and 2 bar cases by performing seven simulations with [CCN] set to $10^2, 10^3, \ldots, 10^7, 10^8$ kg^{-1} (see Section 4.3). The primary effect of decreasing [CCN] is to increase the size of the cloud particles when they form. On the one hand, this enhances the sedimentation rate and thus decreases the mass of the cloud (and thus its opacity). On the other hand, for a given cloud mass, this affects the cloud opacity by changing the number of particles and their single scattering properties. We found that the first effect dominates: almost no clouds are present with [CCN] = 10^2 kg^{-1}. With higher [CCN], the average cloud mass increased by a factor of about 3 for each order of magnitude increase in [CCN]. Meanwhile, the mean cloud particle sizes (computed by taking into account sedimentation and sublimation below the condensation level) remains near 10–20 μm. As a result, with $Ps = 2$ bar, the mean cloud optical depth reaches 16, 67 and 156 for [CCN] = 10^6, 10^7 and 10^8 kg^{-1}, respectively. In the last two cases, the cloud optical depth is too thick to allow the scattering greenhouse effect to take place (Forget and Pierrehumbert, 1997). The clouds are so thick in the visible that albedo increases outweigh the scattering of upwelling IR. The clouds reflect most of the incoming solar radiation, and their net effect is to cool the surface as seen in Fig. 13. With $Ps = 0.5$ bar, the mass of CO_2 ice clouds is lower and the cloud warming is maximized with more nuclei, up to 10^7 kg^{-1} (Fig. 13).

5.3.2. Supersaturation

As mentioned in Section 2, based on the measured constraints on the critical saturation level and the microphysical properties of the formation of carbon dioxide cloud particles (Glandorf et al., 2002), Colaprete and Toon (2003) pointed out that, since nucleation efficiency decreases when the size of the nucleating particles decreases, only the biggest particles are efficiently nucleated and are able to condensate CO_2. They concluded that, as a result, CO_2 clouds on early Mars should contain few, large particles with average radii greater than 500 μm. In addition, they showed that a supersaturation of nearly 35% is needed to allow for such an efficient nucleation.

While the first effect could be well mimicked by reducing [CCN] as done above, we have run another set of simulations to quantify the impact of the critical supersaturation needed to form clouds in a cloud free medium. In these simulations, the number density of CCN is prescribed as above. However, in a grid cell where no significant amount of carbon dioxide ice is present at the beginning of a timestep, CO_2 is allowed to condensate only if the saturation $s = p/p_{sat}$ reaches a critical value $s_{crit} = 1.35$, i.e. if the temperature in the cell is below the nucleation temperature $T_{nuc}(p) = T_c(p/s_{crit})$, where $T_c(p)$ is the equilibrium condensation temperature for a CO_2 partial pressure p.

The average temperatures reached in these simulations are also shown in Fig. 13 as a function of [CCN]. As can be seen, the need for supersaturation decreases the warming effect of CO_2 clouds by a few degrees. However, this variation is weaker than the one obtained by varying the density of CCN.

5.4. Impact of obliquity and orbital parameters

The obliquity and the eccentricity of Mars have strongly varied throughout its existence. As the evolution of these parameters is

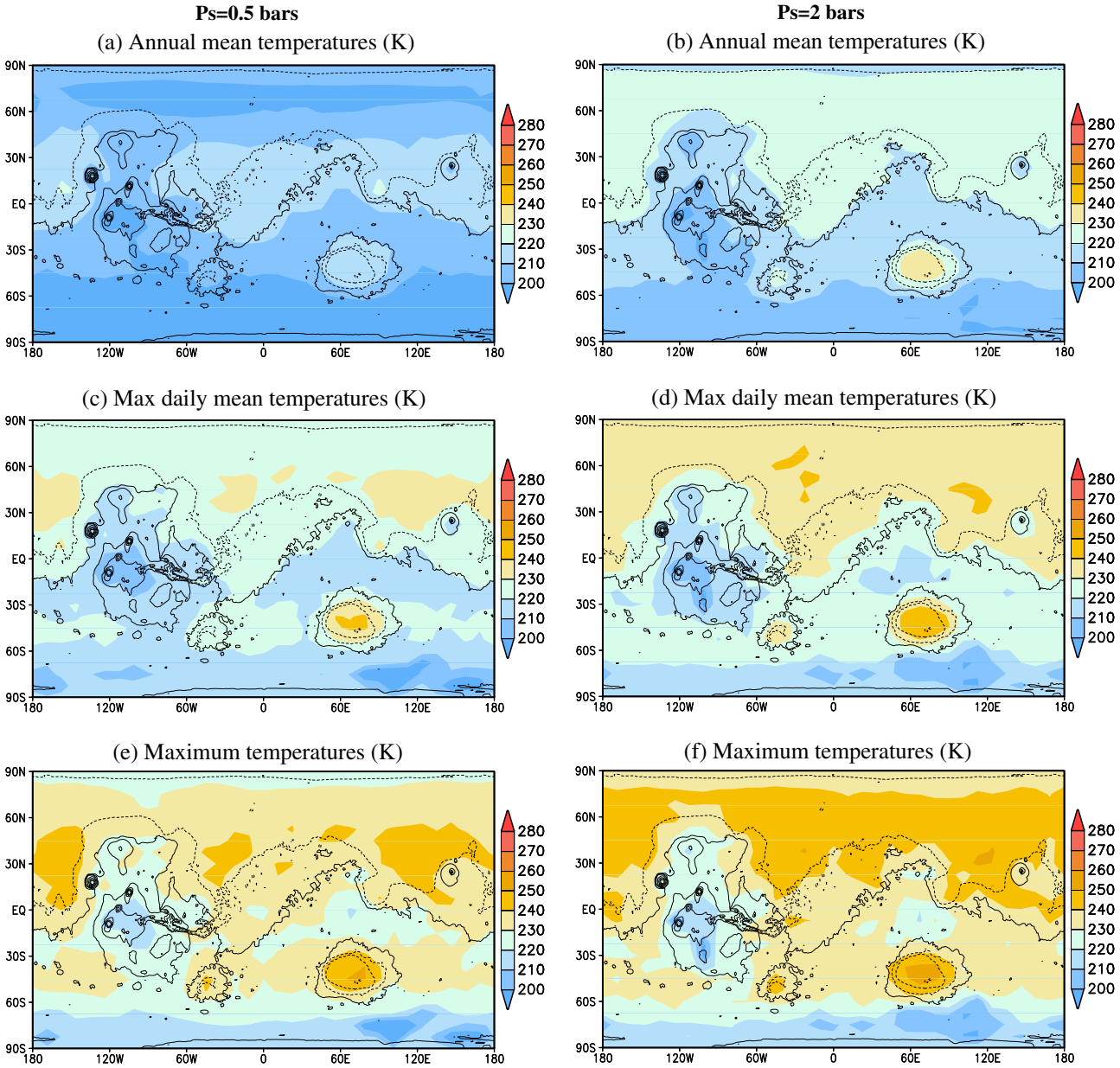

Fig. 8. Same as Fig. 6, but for an "ice-covered" Mars, in which the ground albedo and thermal inertia are set to 0.4 and 1000 J $s^{-1/2}$ m^{-2} K^{-1} everywhere.

strongly chaotic, it is not possible to know their values before a few million years ago (Laskar et al., 2004). Nevertheless, Laskar et al. (2004) showed that the obliquity could have varied between less than 5° and up to more than 60° or even 70°. In fact, the average value of the obliquity over 5 Gyr was estimated to be 37.625° with a standard deviation of 13.82°. The average eccentricity was 0.0690, with standard deviation 0.0299. More recently, Brasser and Walsh (2011) reanalyzed the stability of the martian obliquity for the Noachian era, taking into account the fact that before the late heavy bombardment the giant planets may have been on drastically different orbits than today, according to Gomes et al. (2005). For such conditions, they found that the martian obliquity would have remained chaotic for its most probable mean values, between about 30° and 60°, but more stable for the less probable mean obliquities below 30° (with oscillation amplitude still as high as 20°) and above 60° (with amplitude of 9°).

Varying the obliquity or the season of perihelion in models of the present-day Mars climate system has a profound impact on the surface temperatures and the water cycle (e.g. Haberle et al., 2003; Forget et al., 2006; Montmessin et al., 2007a). The impact is especially strong at high latitudes, with the average insolation at the pole proportional to the sine of the obliquity. The permanent polar caps predicted to form for $Ps = 0.1$ and $Ps = 0.3$ bar in the baseline case (25° obliquity) and discussed in Section 5.1 do not form at 35° obliquity. Conversely, we found that a southern permanent polar cap forms when running with $Ps = 0.5$ bar and 10° obliquity (whereas there is no such cap in the baseline case with 25° obliquity shown in Fig. 3c). With $Ps = 2$ bar, the thick atmosphere prevents the formation of permanent polar caps even in the 10° obliquity case. In fact, in that simulation CO_2 does not condense on the surface at all! Fig. 14 summarizes the range of mean surface pressures and obliquities for which permanent CO_2 ice caps are predicted to form, possibly leading to atmospheric collapse.

In general, a higher obliquity corresponds to a stronger seasonal cycle, with a warmer summer and a colder winter at mid and high latitudes. Could this significantly increase maximum temperatures

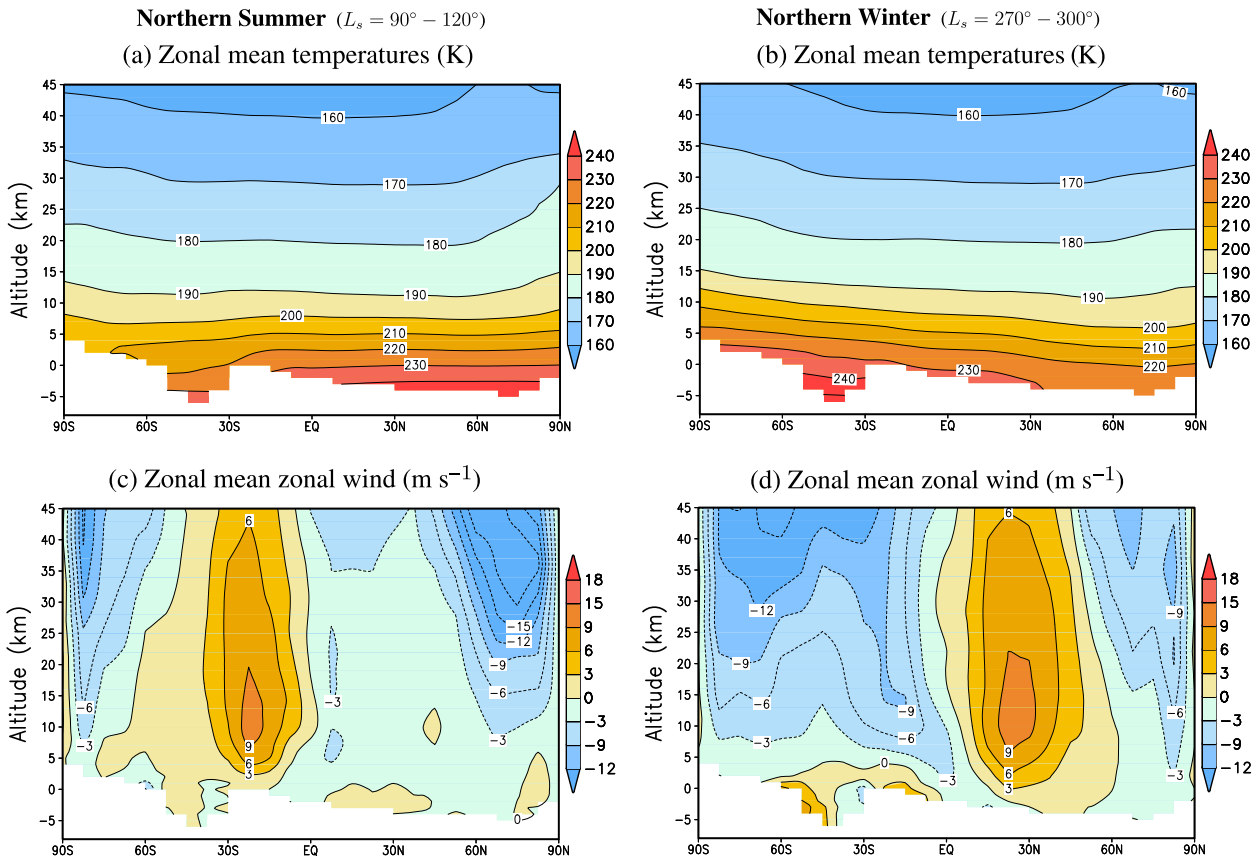

Fig. 9. Time-mean section of zonal-mean temperature (K) and zonal wind (m s^{-1}) for two opposite seasons in our baseline simulation with mean surface pressure 2 bar (obliquity = 25°, [CCN] = 10^5 kg^{-1}, circular orbit). The white areas represent grid points below the surface.

and allow seasonal melting? Fig. 15 shows the global mean, maximum daily mean and planetary maximum temperatures in the *Ps* = 0.5 and 2 bar cases for various obliquities between 10° and 60°. In both cases, the global mean temperature slightly decreases with obliquity. This is due to the raising of the albedo resulting from the seasonal polar caps which are more and more extensive when obliquity increases. As expected, the maximum daily mean temperature strongly increases with obliquity, especially in the *Ps* = 0.5 bar case for which temperature above 0 °C are predicted at very high obliquity. Looking at temperature maps (not shown), we can see that such high temperatures are reached in both hemisphere (more in the north), above about 70° latitude.

Insolation can be further increased near perihelion in the case of an eccentric orbit. To explore this effect, and in order to create a realistic "optimum case" we performed two additional simulations with *Ps* = 0.5 and 2 bar, assuming an eccentricity of 0.1, a perihelion during northern summer solstice, and an obliquity set to 41.8° (the most likely obliquity for Mars according to Laskar et al. (2004)). The corresponding maximum daily mean temperatures are shown in Fig. 16. In the 0.5 bar case, seasonal temperatures above 0 °C are predicted everywhere above 70° latitude. If valley networks and layered deposits were mostly observed at such high latitudes, it would be interesting to relate their formation to this type of orbital configurations. Of course, this is not the case.

5.5. Impact of atmospheric dust

To explore the radiative effects of airborne mineral aerosols, we have used the dust parameterization described in Section 4.4 and performed a series of simulations with various amount of dust in the *Ps* = 0.5 and 2 bar cases. The impact of dust opacity on the global averaged surface temperature is shown in Fig. 17. Two vertical distributions are employed. When the"dust top" is set to 100 km, the dust mixing ratio decreases slowly in the lower 50 km (80% of the surface value at 50 km) and more steadily above, up to 100 km. Similarly, with a dust top at 30 km, most of the dust is confined below 20 km.

In most cases, it is found that dust can slightly warm the surface. With a dust visible opacity τ set to $\tau = 5$, surface temperatures are increased by a couple of kelvins in the *Ps* = 0.5 bar case, and by more than 10 K with *Ps* = 2 bar. With dust opacity $\tau = 10$, the impact is reduced. To interpret these results, we can note that airborne dust modifies the energy balance in four ways: (1) Dust absorbs solar radiation and thus warms the atmosphere, (2) as a result, it decreases the CO_2 ice clouds opacity, (3) Dust decreases the planetary albedo, and (4) Dust increases the atmospheric infrared opacity. The first two effects tend to reduce the atmospheric greenhouse surface warming and thus the mean surface temperatures. However, the other two effects work in the opposite direction and actually dominate. Fig. 18 illustrates the impact of dust on the temperature profiles in the *Ps* = 2 bar case. Temperatures above 10 km are warmed by 15 K with an opacity $\tau = 5$ and by more than 20 K with $\tau = 10$. This should decrease the greenhouse effect by increasing the outgoing infrared radiation, but this is more than compensated by the fact that the dust infrared opacity allows the mean infrared emission to take place at higher and colder altitude. The dominant effect is thus an increase in surface temperature to keep the energy budget in balance. This is less true with $\tau = 10$, and one can see that the surface temperature is then lower than with $\tau = 5$. In the $\tau = 5$ case, the CO_2 ice cloud mean opacity is reduced from about 5 with no dust down to about 1.5

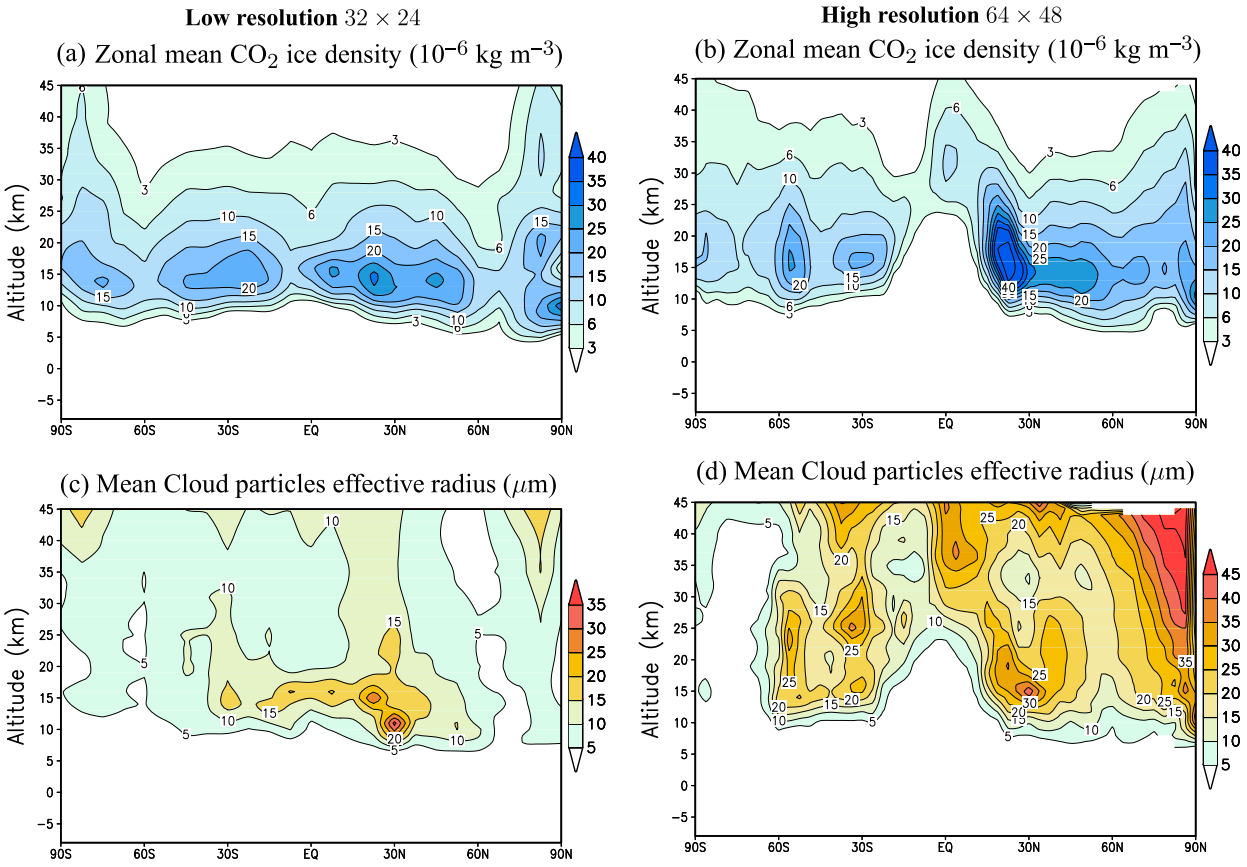

Fig. 10. Annual-mean section of zonal-mean CO_2 ice cloud density and particle radius, for two simulations with different horizontal resolution (mean surface pressure 2 bar, obliquity = 25°, [CCN] = 10^5 kg^{-1}, circular orbit). Particle radii are averaged with a relative weight proportional to the CO_2 ice mixing ratio.

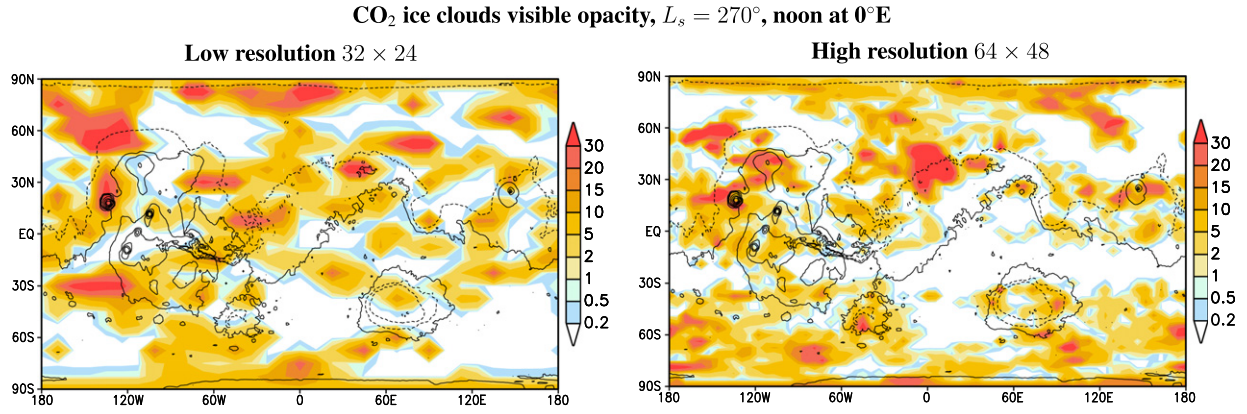

Fig. 11. An example of the instantaneous CO_2 ice clouds coverage for two simulations with different horizontal resolution (mean surface pressure 2 bar, obliquity = 25°, [CCN] = 10^5 kg^{-1}, circular orbit).

and 0.17 with the dust top at 30 and 100 km, respectively. The colder upper atmosphere temperatures and the thicker clouds explain why surface temperatures are a few kelvins warmer when the dust is confined in the lower atmosphere.

5.6. Role of water

In this paper we have assumed that Mars was mostly dry, and neglected the additional greenhouse effect of water vapor. However, even in the case of a water-covered Mars, this effect is limited because our predicted atmospheric temperatures are in most cases so low that even at saturation the concentration of water vapor remains small.

In the companion paper, Wordsworth et al. (2012) present simulations similar to our baseline cases with various CO_2 surface pressure, but in which the greenhouse effect of water vapor is maximized by assuming 100% relative humidity everywhere. As seen on their Figs. 2 and 3, it is found that even in this overestimated case, water vapor only increases surface temperatures by a few kelvins, and thus does not qualitatively change our conclusions. In reality, water also affects the climate by forming water ice clouds which can either cool or warm the planet. This is further discussed in Wordsworth et al. (2012).

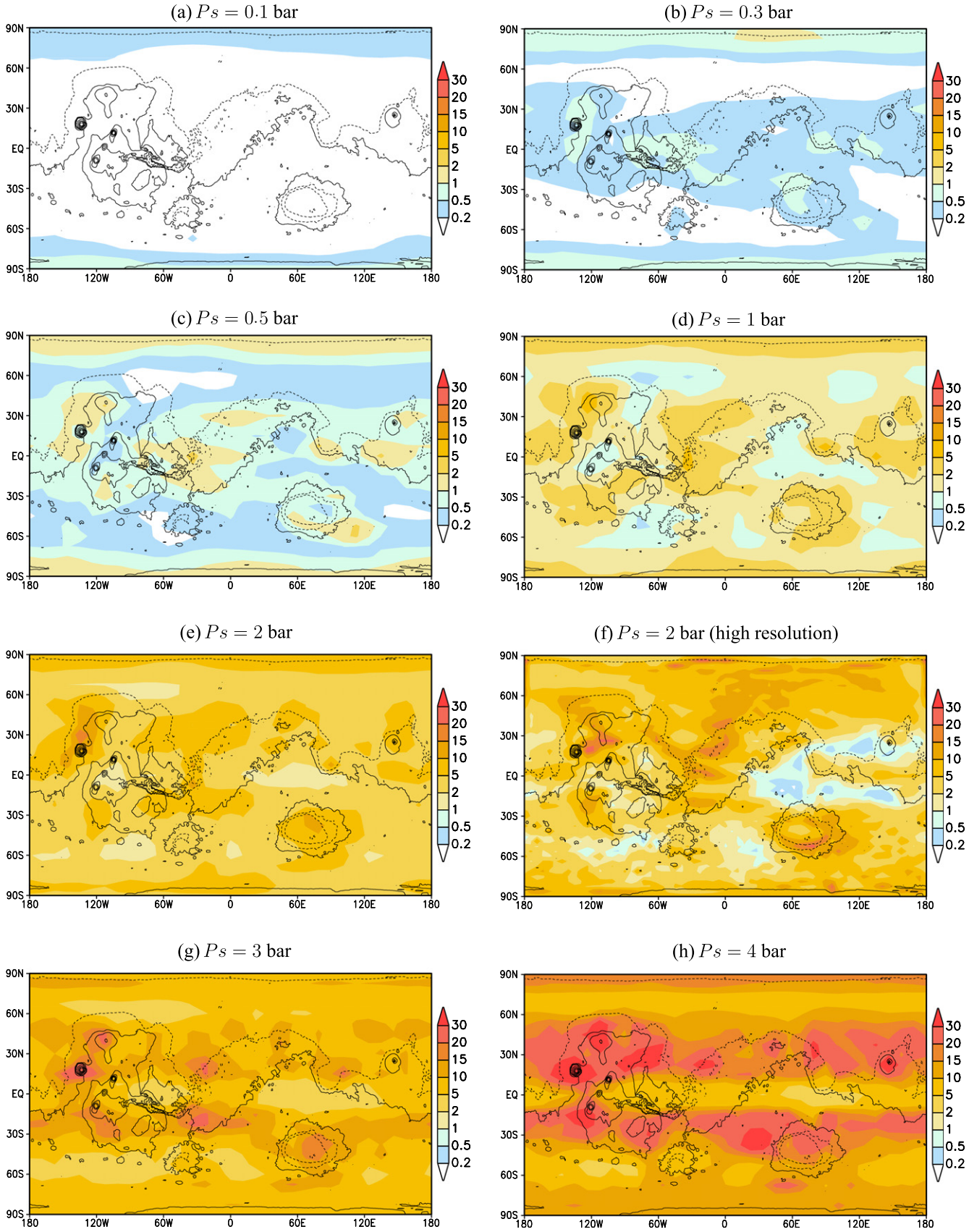

Fig. 12. Map of annual mean CO_2 ice cloud optical depth for various mean surface pressure *Ps* (obliquity = 25°, [CCN] = 10^5 kg^{-1}, circular orbit).

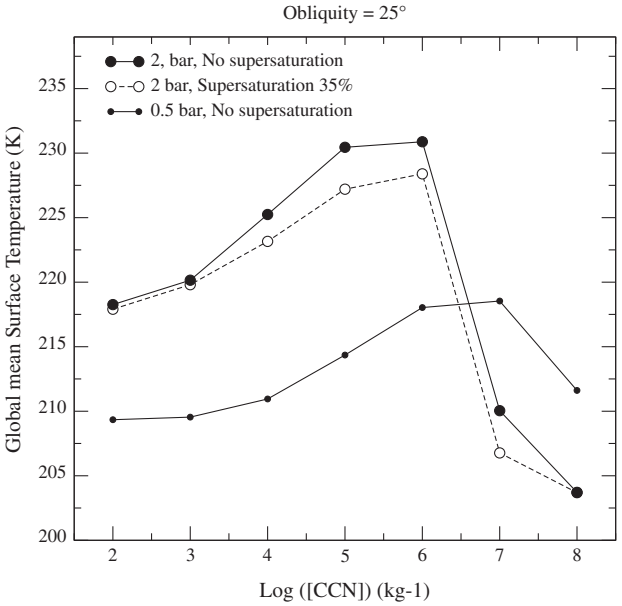

Fig. 13. Global annual averaged surface temperature (K) as a function of cloud condensation nuclei number mixing ratio (kg^{-1}) in the 2 bar mean surface pressure cases (obliquity = 25°, circular orbit), and assuming either no supersaturation or a 35 % supersaturation to form CO_2 ice clouds (see text).

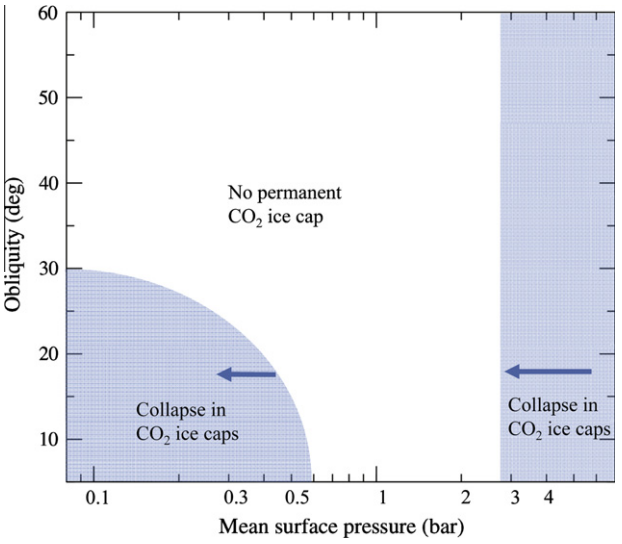

Fig. 14. Schematic drawing illustrating the range of mean surface pressures and obliquities for which permanent CO_2 ice caps are predicted to form after 10 years of simulations. It is based on model runs performed combining pressure values of 0.1, 0.3, 0.5, 1, 2, 3, 4 bars and obliquities of 10°, 25°, 35° and 45° to explore the parameters space. The sensitivity to other model parameters is not shown. In particular, as in all simulations in this paper, the CO_2 ice albedo and emissivity were set to 0.5 and 0.85 respectively, but one can expect that the figure would be different assuming other CO_2 ice radiative properties. The arrows illustrate the fact that when permanent CO_2 ice forms a part of the atmosphere may collapse and the pressure decrease below the initial value.

6. Discussion and conclusion

6.1. Early Mars climate with a CO_2 atmosphere would have been cold

In this work, our purpose has been to develop a climate model complete enough to properly answer the question "what is the climate on a Mars-like planet with a thick CO_2 atmosphere and a faint young Sun?" Previous work had found contradictory answers to this apparently simple question (Pollack et al., 1987; Kasting, 1991; Forget and Pierrehumbert, 1997; Mischna et al., 2000; Colaprete and Toon, 2003). By using a complete 3D GCM, revised spectroscopic properties for collision-induced CO_2, and by systematically exploring the model sensitivity to the possible surface pressures, cloud microphysics properties, obliquity and orbital properties, atmospheric dust loading and model resolution, we hope to have provided an improved answer to the question.

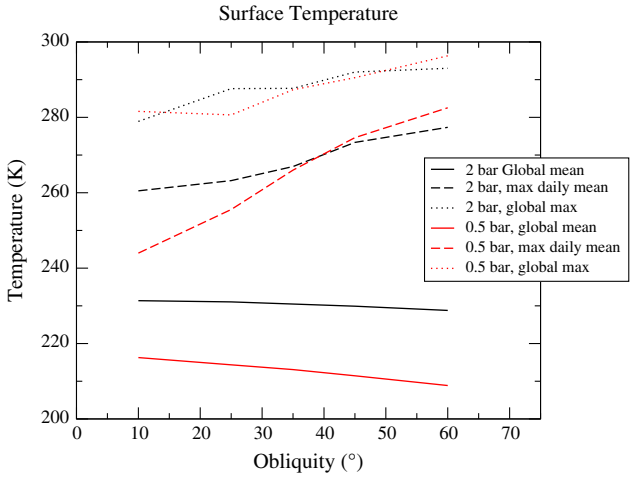

Fig. 15. Surface temperature statistics (K) as a function of obliquity in the 0.5 and in the 2 bar mean surface pressure cases (circular orbit).

In our simulations, a wide range of dynamical, meteorological and climatic phenomenons are observed. Unlike on present day Mars, and more like on the Earth, for pressure higher that a fraction of bar, surface temperatures varies with altitude because of the adiabatic cooling and warming of the atmosphere when it moves vertically and the increased coupling between the atmosphere and the surface under higher atmospheric pressures than today. In most simulations, CO_2 ice clouds cover a major part of the planet but not all. Their behavior is controlled by a combination of large scale ascents and descents of air, stationary and travelling waves, and resolved gravity waves related to the topography. The formation of CO_2 ice seasonal or perennial deposits is also a key process in the climates that we have explored. In particular, atmospheric collapse in permanent CO_2 ice caps could have buffered the thickness of the early Mars atmosphere to pressures lower than about 3 bar (in the unlikely case that enough CO_2 was available; see Section 3). Conversely at pressures lower than 1 bar, we find that if the obliquity is lower than a threshold value between about 10° and 30° (depending on the initial pressure), a part of the atmosphere may be trapped in the high latitudes, as on Mars today. However, as mentioned above, to properly simulate an equilibrated atmosphere/permanent CO_2 ice cap system, it would also be necessary to take into account the ability of CO_2 ice glaciers to flow and spread, and probably include the effect of slopes and roughness (Kreslavsky and Head, 2011).

Our most striking result is that no combination of parameters can yield surface temperatures consistent with the melting and flow of liquid water as suggested by the available geological evidence on early Mars. Previous studies had suggested that CO_2 ice clouds could have strongly warmed the planet thanks to their scattering greenhouse effect. Looking at Figs. 1 and 13, one can see that the optimum case exhibiting maximum surface temperatures in our simulations is with $Ps = 2$ bar and [CCN] near 10^5–10^6 kg^{-1}. This actually corresponds to one of the reference cases that we have studied in detail. Even in that case, the mean cloud warming remains lower than 15 K because of the partial cloud coverage and

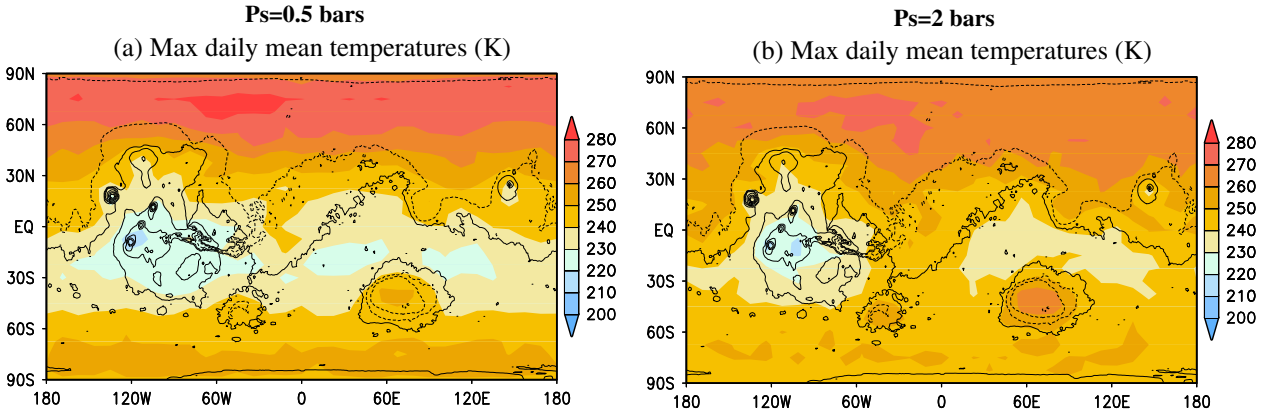

Fig. 16. Maximum daily mean surface temperatures (K) obtained with simulations with a 41.8° obliquity, eccentricity of 0.1, and Mars closest to the Sun in Northern summer (L_s = 90° at perihelion). This illustrates the warmest daily mean surface temperatures that can be obtained in our simulations with surface pressure of 0.5 and 2 bars.

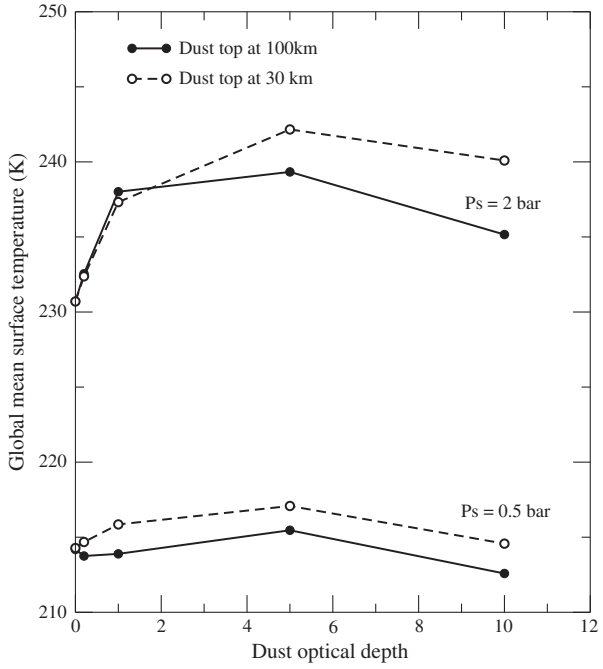

Fig. 17. Global mean surface temperature (K) as a function of dust opacity in the 0.5 and in the 2 bar mean surface pressure cases (circular orbit).

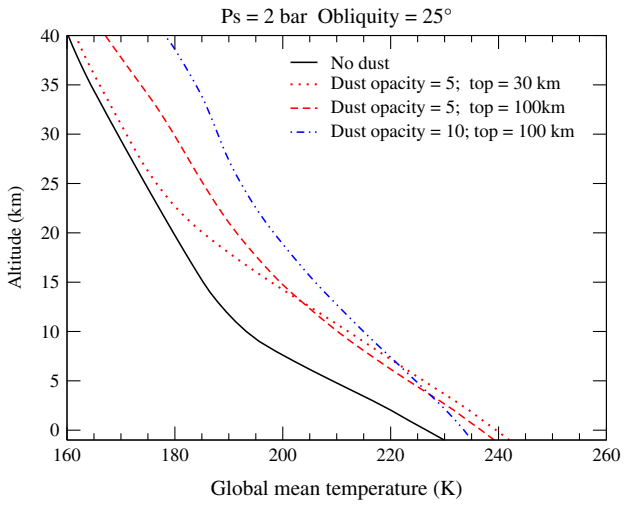

Fig. 18. Global average temperature profile in the 2 bar mean surface pressure case, and with varying dust loading and vertical distribution.

the limited cloud optical depth. We conclude that a CO_2 atmosphere could not have raised the annual mean temperatures above 0 °C anywhere on the planet. Summertime diurnal mean surface temperatures above 0 °C (a condition which could have allowed rivers and lakes to form) are predicted for obliquity larger than 40° at high latitudes but not in locations where most valley networks or layered sedimentary units are observed. At most latitudes, above melting temperatures occur, but only for a few hours during summer afternoons, and assuming albedo and thermal inertia values which may be unrealistic for snow or ice deposits. In the companion paper, Wordsworth et al. (2012) present further results on this subject using a full water cycle model that predicts the stability and evolution of surface ice deposits.

6.2. Was the early Sun brighter than expected?

Like in most previous model studies, we assumed that the early solar flux was 75% than today, on the basis of the "standard solar model" (e.g. Gough, 1981). Can this model be questioned? The fundamental reason is very robust: "The gradual increase in luminosity during the core hydrogen burning phase of evolution of a star is an inevitable consequence of Newtonian physics and the functional dependence of the thermonuclear reaction rates on density, temperature and composition" (Gough, 1981). In practice, it agrees very well with solar neutrinos and helioseismology observations. The only way to explain a brighter early Sun is to assume that it was more massive initially and that it subsequently lose the excess mass in an intense solar wind during its first billion years (Whitmire et al., 1995). A few percent of the mass would be sufficient because a star luminosity strongly depends on its mass. Interestingly, a younger more massive Sun has also been suggested recently to explain inconsistencies between the standard solar model predictions and recently revised measurements of the solar elemental abundances (Guzik and Mussack, 2010; Turck-Chièze et al., 2011). However, observations of mass loss in young stars do not suggest that they lose significant mass after the first 0.1 Gyr (Wood et al., 2005; Minton and Malhotra, 2007). Nonetheless, the faint young Sun is still a topic of active investigation.

6.3. Other greenhouse gases?

Could supplemental trace greenhouse gases boost the greenhouse power of a pure CO_2 (and H_2O) atmosphere? Past studies

have notably explored the effects of sulfur dioxide (SO_2), hydrogen sulfide (H_2S), methane (CH_4), and ammonia (NH_3). The key to the success of these gases in solving the faint young Sun paradox for early Mars rests on two main conditions: their ability to absorb infrared radiation in parts of the spectrum not covered by CO_2 and H_2O, and their ability to sustain the needed concentrations given plausible sources and sinks.

Of the gases listed, NH_3 has the potential to plug up the so-called window region (800–1200 cm^{-1}) as it exhibits strong absorption between 700 and 1300 cm^{-1}. This makes it a very powerful greenhouse gas. Kasting et al. (1992) suggested that 500 ppm of NH_3 in a 4–5 bar CO_2 atmosphere could raise surface temperatures to 273 K. However, NH_3 is photochemically unstable (Kuhn and Atreya, 1979) and would require shielding to survive (e.g., Sagan and Chyba, 1997; Wolf and Toon, 2010). Methane, which is also unstable and whose photolysis products could provide the shield, has absorption features at somewhat higher wavenumbers (1200–1500 cm^{-1}), which could further help reduce the outgoing infrared. However, recent calculations indicate that even at concentrations of 500 ppm CH_4 does not significantly boost the greenhouse effect of a pure CO_2/H_2O atmosphere (Ramirez and Kasting, 2011). This is partly the result of an overlap with water bands, partly because these bands are on the wings of the Planck function, and partly due to the fact that CH_4 also absorbs in the near infrared, which has an anti-greenhouse effect. And like NH_3, CH_4 would require strong sources to sustain the above concentrations.

As noted in the Introduction, the detection of Noachian–Hesperian aged sulfate deposits has renewed interest in SO_2 and H_2S as potential greenhouse gases. An obvious source for these gases is volcanic activity, which was much higher in the past than it is today. H_2S has absorption features in the window region but they are weak, and its stronger bands at lower wavenumbers occur at the tail end of the Planck function. On the other hand, SO_2 ν_2 fundamental near 520 cm^{-1} is near the peak of a 273 K Planck function, and it also has significant opacity at the high wavenumber end of the window region. Thus, SO_2 has received most of the attention (e.g., Halevy et al., 2007; Johnson et al., 2008).

To be effective, SO_2 needs to build up to concentrations around the 10 ppm level or higher in moderately thick atmospheres (surface pressures greater than 0.5 bar). In the model of Johnson et al. (2008) global mean surface temperatures well above freezing are achieved with SO_2 concentrations in this range. This is the only modern model to predict such warm conditions with a pure gaseous greenhouse effect. However, in practice the SO_2 greenhouse faces significant challenges as SO_2 readily converts to aerosols regardless of the redox state of the atmosphere. And as on Earth, these aerosols should have a net cooling effect on surface temperatures (Tian et al., 2010). Furthermore, SO_2 is highly soluble and will washout quickly when conditions become warm enough for rainfall.

Thus, while the supplemental greenhouse gases considered thus far in the literature cannot be ruled out, they require special circumstances to play a significant role in warming the surface of Mars to the melting point of liquid water. To date, no model has been published that convincingly demonstrates a gaseous greenhouse can solve the faint young Sun problem for early Mars. Within that context, using our Global Climate Model, we plan to explore the radiative effect and the chemical cycle of these gases, starting with the sulfur cycle.

6.4. A cold early Mars warmed episodically and locally?

The idea that early Mars climate may have been cold is not new. Several studies have suggested that the geomorphological evidence related to liquid water could be explained by assuming hydrothermal convection and the formation of aquifers driven by geothermal heat and heat associated with impacts (Squyres and Kasting, 1994; Gaidos and Marion, 2003). Erosion and surface alteration may have occurred by saline and acidic liquid solutions (brines) which can be stable at sub-zero temperatures (Fairén, 2010). Impacts may have induced melting and rainfall on a global scale (Toon et al., 2010) or locally (e.g. Mangold, 2012, and reference therein) which may explain the formation of fluvial valleys even under cold background climate conditions. Similarly, while clay minerals have been thought to be an indication of surface weathering by liquid water and thus an indication of warm and wet past conditions, Ehlmann et al. (2011) showed that, in many locations, available data instead indicates clay formation by hydrothermal groundwater circulation possibly operating in cold, arid surface conditions. Furthermore, Meunier et al. (2012) proposed that the iron-and-magnesium-rich clay formed directly by the precipitation from water-rich magama-derived fluids.

This new paradigm is not without problems. In particular, it is more and more clear that "early" Mars encompasses several epochs. While a cold early planet scenario may be consistent with relatively recent late Noachian or Hesperian geological features such as delta fans or the most recent fluvial features, several authors have argued that it could not explain the morphology of large valley networks, the very high global erosion rate inferred for the early Noachian period, or the formation of extensive deposits of phyllosilicates like in the Mawrth Vallis region (e.g. Craddock and Howard, 2002; Bibring et al., 2006; McKeown et al., 2009).

In any case, there is no doubt that conditions on Mars during the first billion years of its history were dramatically different from those at present. A thicker atmosphere was probably necessary to allow water to flow for long distances across the surface. Our simulations of the resulting climate provide clues on the environment, and notably show that with surface pressure above a fraction of a bar, the southern highlands become cold traps where ice may migrate and replenish water sources. This hydrological cycle is modelled and discussed in detail in the companion paper (Wordsworth et al., 2012).

Acknowledgments

We are grateful for the comments on the text and scientific suggestions provided by James W. Head. We thank N. Mangold, B. Charnay, F. Leblanc, A. Spiga, J.-P. Bibring for helpful discussions. We also appreciate the reviews provided by E. Kite and S. Clifford.

References

Andreae, M.O., 2009. Correlation between cloud condensation nuclei concentration and aerosol optical thickness in remote and polluted regions. Atmos. Chem. Phys. 9, 543–556.
Barabash, S., Fedorov, A., Lundin, R., Sauvaud, J.-A., 2007. Martian atmospheric erosion rates. Science 315, 501–503.
Baranov, Y.I., Lafferty, W.J., Fraser, G.T., 2004. Infrared spectrum of the continuum and dimer absorption in the vicinity of the O_2 vibrational fundamental in O_2/CO_2 mixtures. J. Mol. Spectrosc. 228, 432–440.
Bibring, J.-P. et al., 2005. Mars surface diversity as revealed by the OMEGA/Mars Express observations. Science 307, 1576–1581.
Bibring, J.-P. et al., 2006. Global mineralogical and aqueous Mars history derived from OMEGA/Mars Express data. Science 312, 400–404.
Boynton, W.V. et al., 2009. Evidence for calcium carbonate at the Phoenix Landing Site. Science 325, 61.
Brasser, R., Walsh, K.J., 2011. Stability analysis of the martian obliquity during the Noachian era. Icarus 213, 423–427.
Carr, M.H., 1996. Water on Mars. Oxford University Press, New York.
Chassefière, E., Leblanc, F., 2004. Mars atmospheric escape and evolution; interaction with the solar wind. Planet. Space Sci. 52, 1039–1058.
Colaprete, A., Toon, O.B., 2003. Carbon dioxide clouds in an early dense martian atmosphere. J. Geophys. Res. (Planets), 1–6.
Craddock, R.A., Maxwell, T.A., 1993. Geomorphic evolution of the martian highlands through ancient fluvial processes. J. Geophys. Res. 98, 3453–3468.
Craddock, R.A., Howard, A.D., 2002. The case for rainfall on a warm, wet early Mars. J. Geophys. Res. (Planets) 107, 1–21.

Demott, P.J. et al., 2003. Measurements of the concentration and composition of nuclei for cirrus formation. Proc. Natl. Acad. Sci. 100, 14655–14660.
Durham, W.B., Kirby, S.H., Stern, L.A., 1999. Steady-state flow of solid CO_2: Preliminary results. Geophys. Res. Lett. 26, 3493–3496.
Ehlmann, B.L. et al., 2008. Orbital identification of carbonate-bearing rocks on Mars. Science 322, 1828–1832.
Ehlmann, B.L. et al., 2011. Subsurface water and clay mineral formation during the early history of Mars. Nature 479, 53–60.
Fairén, A.G., 2010. A cold and wet Mars. Icarus 208, 165–175.
Fanale, F.P., Salvail, J., Banerdt, W.B., Saunders, R.S., 1982. Mars: The regolith–atmosphere–cap system and climate change. Icarus 50, 381–407.
Fassett, C.I., Head, J.W., 2008. The timing of martian valley network activity: Constraints from buffered crater counting. Icarus 195, 61–89.
Forget, F., Pierrehumbert, R.T., 1997. Warming early Mars with carbon dioxide clouds that scatter infrared radiation. Science 278, 1273–1276.
Forget, F., Hourdin, F., Talagrand, O., 1998. CO_2 snow fall on Mars: Simulation with a general circulation model. Icarus 131, 302–316.
Forget, F. et al., 1999. Improved general circulation models of the martian atmosphere from the surface to above 80 km. J. Geophys. Res. 104, 24155–24176.
Forget, F., Haberle, R.M., Montmessin, F., Levrard, B., Head, J.W., 2006. Formation of glaciers on Mars by atmospheric precipitation at high obliquity. Science 311, 368–371.
Forget, F. et al., 2009. Density and temperatures of the upper martian atmosphere measured by stellar occultations with Mars Express SPICAM. J. Geophys. Res. (Planets) 114, E01004.
Gaidos, E., Marion, G., 2003. Geological and geochemical legacy of a cold early Mars. J. Geophys. Res. (Planets) 108, 5055.
Gendrin, A. et al., 2005. Sulfates in martian layered terrains: The OMEGA/Mars Express view. Science 307, 1587–1591.
Glandorf, D.L., Colaprete, A., Tolbert, M.A., Toon, O.B., 2002. CO_2 snow on Mars and early Earth: Experimental constraints. Icarus 160, 66–72.
Gomes, R., Levison, H.F., Tsiganis, K., Morbidelli, A., 2005. Origin of the cataclysmic late heavy bombardment period of the terrestrial planets. Nature 435, 466–469.
González-Galindo, F., Bougher, S.W., López-Valverde, M.A., Forget, F., Murphy, J., 2010. Thermal and wind structure of the martian thermosphere as given by two General Circulation Models. Planet. Space Sci. 58, 1832–1849.
Gough, D.O., 1981. Solar interior structure and luminosity variations. Solar Phys. 74, 21–34.
Grott, M., Morschhauser, A., Breuer, D., Hauber, E., 2011. Volcanic outgassing of CO_2 and H_2O on Mars. Earth Planet. Sci. Lett. 308, 391–400.
Gruszka, M., Borysow, A., 1998. Computer simulation of the far infrared collision induced absorption spectra of gaseous CO_2. Mol. Phys. 93, 1007–1016.
Gumbel, J., Megner, L., 2009. Charged meteoric smoke as ice nuclei in the mesosphere. Part 1: A review of basic concepts. J. Atmos. Solar-Terr. Phys. 71, 1225–1235.
Guzik, J.A., Mussack, K., 2010. Exploring mass loss, low-Z accretion, and convective overshoot in solar models to mitigate the solar abundance Problem. Astrophys. J. 713, 1108–1119.
Haberle, R.M., 1998. Early Mars climate models. J. Geophys. Res. 103, 28467.
Haberle, R.M., Murphy, J.R., Schaeffer, J., 2003. Orbital change experiments with a Mars general circulation model. Icarus 161, 66–89.
Haberle, R.M. et al., 2008. The effect of ground ice on the martian seasonal CO_2 cycle. Planet. Space Sci. 56, 251–255.
Halevy, I., Zuber, M.T., Schrag, D.P., 2007. A sulfur dioxide climate feedback on early Mars. Science 318, 1903–1907.
Hansen, G.B., 2005. Ultraviolet to near-infrared absorption spectrum of carbon dioxide ice from 0.174 to 1.8 μm. J. Geophys. Res. (Planets) 110, E11003.
Hansen, J.E., Travis, L.D., 1974. Light scaterring in planetary atmosphere. Space Sci. Rev. 16, 527–610.
Harvey, R.P., 2010. Carbonates and martian climate. Science 329, 400–401.
Hirschmann, M.M., Withers, A.C., 2008. Ventilation of CO_2 from a reduced mantle and consequences for the early martian greenhouse. Earth Planet. Sci. Lett. 270, 147–155.
Ho, W., Birnbaum, G., Rosenberg, A., 1971. Far-infrared collision-induced absorption in CO_2 I. Temperature dependence. J. Comput. Phys. 55, 1028–1038.
Hourdin, F., Armengaud, A., 1999. Test of a hierarchy of finite-volume schemes for transport of trace species in an atmospheric general circulation model. Mon. Weather Rev. 127, 822–837.
Hourdin, F., Forget, F., Talagrand, O., 1995. The sensitivity of the martian surface pressure to various parameters: A comparison between numerical simulations and Viking observations. J. Geophys. Res. 100, 5501–5523.
Hourdin, F., Lebonnois, S., Luz, D., Rannou, P., 2004. Titan's stratospheric composition driven by condensation and dynamics. J. Geophys. Res. (Planets) 109, 12005.
Hudson, J.G., Yum, S.S., 2002. Cloud condensation nuclei spectra and polluted and clean clouds over the Indian Ocean. J. Geophys. Res. (Atmos.) 107, 8022–8033.
Johnson, S.S., Mischna, M.A., Grove, T.L., Zuber, M.T., 2008. Sulfur-induced greenhouse warming on early Mars. J. Geophys. Res. (Planets) 113, E08005.
Kasting, J.F., 1991. CO_2 condensation and the early climate of Mars. Icarus 94, 1–13.
Kasting, J.F., Pollack, J.B., Crisp, D., 1984. Effects of high CO_2 levels on surface temperature and atmospheric oxidation state of the early Earth. J. Atmos. Chem. 1, 403–428.
Kasting, J.F., Brown, L.L., Acord, J.M., Pollack, J.B., 1992. Was early Mars warmed by ammonia? In: Haberle, R.M., Jakosky, B.M. (Eds.), Martian Surface and Atmosphere through Time. Lunar Planet. Inst. pp. 84–85.
Kreslavsky, M.A., Head, J.W., 2005. Mars at very low obliquity: Atmospheric collapse and the fate of volatiles. Geophys. Res. Lett. 32, 12202.
Kreslavsky, M.A., Head, J.W., 2011. Carbon dioxide glaciers on Mars: Products of recent low obliquity epochs (?). Icarus 216, 111–115.
Kuhn, W.R., Atreya, S.K., 1979. Ammonia photolysis and the greenhouse effect in the primordial atmosphere of the Earth. Icarus 37, 207–213.
Lammer, H., 2010. Production and loss of the martian CO_2 atmosphere. In: European Planetary Science Congress, September 2010, p. 468.
Lammer, H., Kasting, J.F., Chassefière, E., Johnson, R.E., Kulikov, Y.N., Tian, F., 2008. Atmospheric escape and evolution of terrestrial planets and satellites. Space Sci. Rev. 139, 399–436.
Laskar, J., Correia, A.C.M., Gastineau, M., Joutel, F., Levrard, B., Robutel, P., 2004. Long term evolution and chaotic diffusion of the insolation quantities of Mars. Icarus 170, 343–364.
Leblanc, F., Johnson, R.E., 2002. Role of molecules in pick-up ion sputtering of the martian atmosphere. J. Geophys. Res. (Planets) 22, 10209/2000JE001473.
Lebonnois, S., Hourdin, F., Eymet, V., Crespin, A., Fournier, R., Forget, F., 2010. Superrotation of Venus' atmosphere analyzed with a full general circulation model. J. Geophys. Res. (Planets) 115 (Jun.), 6006.
Lebonnois, S., Burgalat, J., Rannou, P., Charnay, B., 2012. Titan Global Climate Model: A new 3-dimensional version of the IPSL Titan GCM. Icarus 218, 707–722.
Lefèvre, F., Lebonnois, S., Montmessin, F., Forget, F., 2004. Three-dimensional modeling of ozone on Mars. J. Geophys. Res. (Planets) 109, E07004.
Lefèvre, F. et al., 2008. Heterogeneous chemistry in the atmosphere of Mars. Nature 454, 971–975.
Levrard, B., Forget, F., Montmessin, F., Laskar, J., 2004. Recent ice-rich deposits formed at high latitudes on Mars by sublimation of unstable equatorial ice during low obliquity. Nature 431, 1072–1075.
Määttänen, A., Montmessin, F., Gondet, B., Scholten, F., Hoffmann, H., González-Galindo, F., Spiga, A., Forget, F., Hauber, E., Neukum, G., Bibring, J., Bertaux, J., 2010. Mapping the mesospheric CO_2 clouds on Mars: MEx/OMEGA and MEx/HRSC observations and challenges for atmospheric models. Icarus 209, 452–469.
Madeleine, J.-B., Forget, F., Head, J.W., Levrard, B., Montmessin, F., Millour, E., 2009. Amazonian northern mid-latitude glaciation on Mars: A proposed climate scenario. Icarus 203, 390–405.
Madeleine, J.-B., Forget, F., Millour, E., Montabone, L., Wolff, M.J., 2011. Revisiting the radiative impact of dust on Mars using the LMD Global Climate Model. J. Geophys. Res. (Planets) 116, E11010.
Malin, M.C., Edgett, K.S., 2000. Sedimentary rocks of early Mars. Science 290, 1927–1937.
Malin, M.C., Edgett, K.S., 2003. Evidence for persistent flow and aqueous sedimentation on early Mars. Science 302, 1931–1934.
Mangold, N., 2012. Fluvial landforms on fresh impact ejecta on Mars. Planet. Space Sci. 62 (1), 69–85.
Marchant, D.R., Head, J.W., 2007. Antarctic Dry Valleys: Microclimate zonation, variable geomorphic processes, and implications for assessing climate change on Mars. Icarus 192, 187–222.
McKay, C.P., Wharton Jr., R.A., Squyres, S.W., Clow, G.D., 1985. Thickness of ice on perennially frozen lakes. Nature 313, 561–562.
McKeown, N.K. et al., 2009. Characterization of phyllosilicates observed in the central Mawrth Vallis region, Mars, their potential formational processes, and implications for past climate. J. Geophys. Res. (Planets) 114.
Mellor, G.L., Yamada, T., 1982. Development of a turbulence closure model for geophysical fluid problems. Rev. Geophys. 20 (4), 851–875.
Melosh, H.J., Vickery, A.M., 1989. Impact erosion of the primordial atmosphere of Mars. Nature 338, 487–489.
Meunier, A. et al., 2012. Magmatic precipitation as a possible origin of Noachian clays on Mars. Nat. Geosci. 5, 739–743.
Minder, J.R., Mote, P.W., Lundquist, J.D., 2010. Surface temperature lapse rates over complex terrain: Lessons from the Cascade Mountains. J. Geophys. Res. (Atmos.) 115, D14122.
Minton, D.A., Malhotra, R., 2007. Assessing the massive young Sun hypothesis to solve the warm young Earth puzzle. Astrophys. J. 660, 1700–1706.
Mischna, M.A., Kasting, J.F., Pavlov, A., Freedman, R., 2000. Influence of carbon dioxide clouds on early martian climate. Icarus 145, 546–554.
Montmessin, F. et al., 2007a. Hyperspectral imaging of convective CO_2 ice clouds in the equatorial mesosphere of Mars. J. Geophys. Res. (Planets) 112, E11S90.
Montmessin, F., Forget, F., Rannou, P., Cabane, M., Haberle, R.M., 2004. Origin and role of water ice clouds in the martian water cycle as inferred from a general circulation model. J. Geophys. Res. (Planets) 109 (E18), E11S90.
Montmessin, F., Haberle, R.M., Forget, F., Langevin, Y., Clancy, R.T., Bibring, J.-P., 2007b. On the origin of perennial water ice at the south pole of Mars: A precession-controlled mechanism? J. Geophys. Res. (Planets) 112, E08S17.
Moore, J.F., 1971. Infrared Absorption of Carbon Dioxide at High Densities with Application to the Atmosphere of Venus. Tech. Rep. X-630-72-48, NASA Goddard Space Flight Center, Greenbelt, MD.
Morris, R.V. et al., 2010. Identification of carbonate-rich outcrops on Mars by the Spirit rover. Science 329, 421–424.
Osterloo, M.M. et al., 2008. Chloride-bearing materials in the southern highlands of Mars. Science 319, 1651–1654.
Perrin, M.Y., Hartmann, J.M., 1989. Temperature-dependent measurements and modeling of absorption by CO_2–N_2 mixtures in the far line-wings of the 4.3-micron CO_2 band. J. Quant. Spectrosc. Radiat. Transfer 42, 311–317.

Pettengill, G.H., Ford, P.G., 2000. Winter clouds over the north martian polar cap. Geophys. Res. Lett. 27, 609–613.
Pham, L.B.S., Karatekin, Ö., Dehant, V., 2011. Effects of impacts on the atmospheric evolution: Comparison between Mars, Earth, and Venus. Planet. Space Sci. 59, 1087–1092.
Phillips, R.J. et al., 2001. Ancient geodynamics and global-scale hydrology on Mars. Science 291, 2587–2591.
Pollack, J.B., Toon, O.B., Boese, R., 1980. Greenhouse models of Venus' high surface temperature, as constrained by Pioneer Venus measurements. J. Geophys. Res. 85, 8223–8231.
Pollack, J.B., Kasting, J.F., Richardson, S.M., Poliakoff, K., 1987. The case for a wet, warm climate on early Mars. Icarus 71, 203–224.
Postawko, S.E., Kuhn, W.R., 1986. Effect of the greenhouse gases (CO_2, H_2O, SO_2) on martian paleoclimate. J. Geophys. Res. 91, D431–D438.
Poulet, F. et al., 2005. Phyllosilicates on Mars and implications for early martian climate. Nature 438, 623–627.
Ramirez, R.M., Kasting, J.F., 2011. Greenhouse warming on early Mars and extrasolar planets plus a critique of the martian valley impact hypothesis. AGU Fall Meeting Abstracts B4.
Richardson, M.I., Toigo, A.D., Newman, C.E., 2007. PlanetWRF: A general purpose, local to global numerical model for planetary atmospheric and climate dynamics. J. Geophys. Res. 112, E09001.
Rossow, W.B., 1978. Cloud microphysics: Analysis of the clouds of Earth, Venus, Mars, and Jupiter. Icarus 36, 1–50.
Rothman, L.S. et al., 2009. The HITRAN 2008 molecular spectroscopic database. J. Quant. Spectrosc. Radiat. Transfer 110, 533–572.
Sagan, C., Chyba, C., 1997. The early faint young Sun paradox: Organic shielding of ultraviolet-labile greenhouse gases. Science 276, 1217–1221.
Squyres, S., Kasting, J., 1994. Early Mars, how warm and how wet? Science 265, 744–749.
Squyres, S.W., Knoll, A.H., 2005. Sedimentary rocks at Meridiani Planum: Origin, diagenesis, and implications for life on Mars. Earth Planet. Sci. Lett. 240, 1–10.
Squyres, S.W. et al., 2004. In situ evidence for an ancient aqueous environment at Meridiani Planum, Mars. Science 306, 1709–1714.
Squyres, S.W. et al., 2008. Detection of silica-rich deposits on Mars. Science 320, 1063–1067.
Tian, F., Kasting, J.F., Solomon, S.C., 2009. Thermal escape of carbon from the early martian atmosphere. Geophys. Res. Lett. 36, 2205.
Tian, F. et al., 2010. Photochemical and climate consequences of sulfur outgassing on early Mars. Earth Planet. Sci. Lett. 295, 412–418.
Tobie, G., Forget, F., Lott, F., 2003. Numerical simulation of the winter polar wave clouds observed by Mars Global Surveyor Mars Orbiter Laser Altimeter. Icarus 164, 33–49.
Toon, O.B., McKay, C.P., Ackerman, T.P., Santhanam, K., 1989. Rapid calculation of radiative heating rates and photodissociation rates in inhomogeneous multiple scattering atmospheres. J. Geophys. Res. 94, 16287–16301.
Toon, O.B., Segura, T., Zahnle, K., 2010. The formation of martian river valleys by impacts. Annu. Rev. Earth Planet. Sci. 38, 303–322.
Tosca, N.J., Knoll, A.H., 2009. Juvenile chemical sediments and the long term persistence of water at the surface of Mars. Earth Planet. Sci. Lett. 286, 379–386.
Turck-Chièze, S., Piau, L., Couvidat, S., 2011. The solar energetic balance revisited by young solar analogs, helioseismology, and neutrinos. Astrophys. J. 731, L29.
Whitmire, D.P., Doyle, L.R., Reynolds, R.T., Matese, J., 1995. A slightly more massive young Sun as an explanation for warm temperature on early Mars. J. Geophys. Res. 100, 5457–5464.
Wolf, E.T., Toon, O.B., 2010. Fractal organic hazes provided an ultraviolet shield for early Earth. Science 328, 1266–1268.
Wolff, M.J. et al., 2009. Wavelength dependence of dust aerosol single scattering albedo as observed by the Compact Reconnaissance Imaging Spectrometer. J. Geophys. Res. 114, E00D04.
Wood, S.E., 1999. Nucleation and Growth of Carbon Dioxide Ice Crystals in the Martian Atmosphere. Ph.D. Thesis, University of California, Los Angeles.
Wood, B.E., Müller, H.-R., Zank, G.P., Linsky, J.L., Redfield, S., 2005. New mass-loss measurements from astrospheric Lyα absorption. Astrophys. J. 628, L143–L146.
Wordsworth, R., Forget, F., Eymet, V., 2010. Infrared collision-induced and far-line absorption in dense CO_2 atmospheres. Icarus 210, 992–997.
Wordsworth, R., Forget, F., Millour, E., Madeleine, J.-B., Haberle, R.M., Eymet, V., 2011a. Modelling past Mars Climates and water cycle with a thicker CO^2 atmosphere. In: Forget, F., Millour, E. (Eds.), Mars Atmosphere: Modelling and Observation, pp. 447–448.
Wordsworth, R.D., Forget, F., Selsis, F., Millour, E., Charnay, B., Madeleine, J.-B., 2011b. Gliese 581d is the first discovered terrestrial-mass exoplanet in the habitable zone. Astrophys. J. 733, L48.
Wordsworth, R., Forget, F., Millour, E., Head, J.W., Madeleine, J.-B., Charnay, B., 2012. Global modelling of the early Martian climate under a denser CO_2 atmosphere: Water cycle and ice evolution. http://dx.doi.org/10.1016/j.icarus.2012.09.036.
Yung, Y.L., Nair, H., Gerstell, M.F., 1997. NOTE: CO_2 greenhouse in the early martian atmosphere: SO_2 inhibits condensation. Icarus 130, 222–224.
Zahnle, K., Haberle, R.M., Catling, D.C., Kasting, J.F., 2008. Photochemical instability of the ancient martian atmosphere. J. Geophys. Res. (Planets) 113, 11004.